1   Stratospheric circulation response to large Northern high-latitude volcanic eruptions.

2

3   Hera Guðlaugsdóttir[1,2], Yannick Peings[2], Davide Zanchettin[3], Gudrun Magnusdottir[2]

4   [1]University of Iceland, institute of Earth Sciences, 102 Reykjavík, Iceland

5   [2]University of California Irvine, Department of Earth System Science, Irvine CA 92697-3100,

6   United States

7   [3]University Ca'Foscari of Venice, department of Environmental Sciences, Informatics and

8   Statistics, 30123 Venice, Italy

9   *Correspondence to:* Hera Guðlaugsdóttir (hera@hi.is)

10

11

12

13

14   Abstract

15   The temporary enhancement of the stratospheric aerosol layer after major explosive volcanic eruptions can

16   trigger climate anomalies for up to several years following such events. Whereas the mechanisms

17   responsible for the prolonged response to volcanic surface cooling have been extensively investigated for

18   tropical eruptions, less is known about the dynamical response to high-latitude eruptions. Here we use

19   global climate model simulations of an idealized 6 month long northern hemisphere high-latitude eruption

20   to investigate the stratospheric circulation response during the first three post-eruption winters. Two model

21   configurations are used, with an interactive ocean, or with prescribed sea surface temperature. Our results

22   reveal significant differences in the response of the polar stratosphere with an interactive ocean: the surface

23   cooling is enhanced and zonal flow anomalies are stronger in the troposphere, which impacts atmospheric

24   waveguides and upward propagation of large-scale planetary waves. We identify two competing

25   mechanisms contributing to the post-eruption evolution of the polar vortex: 1) A local stratospheric top-

26   down mechanism whereby increased absorption of aerosol-induced thermal radiation yields a polar vortex

27   strengthening via thermal wind response; 2) A bottom-up mechanism whereby anomalous surface cooling

28   yields a wave-activity flux increase that propagates into the winter stratosphere. This causes a weakening

29   of the polar vortex and an increase in the occurrence of sudden stratospheric warming events (SSWs),

30   although with a small signal-to-noise ratio. In the coupled runs, the top-down mechanism dominates over

31   the bottom-up mechanism in winter 1, while the bottom-up mechanism dominates in the follow-up winters.

32

33

Deleted: beyond the duration of the radiative forcing.
Deleted: long-lasting
Deleted: forcing
Deleted: (HL)
Deleted: (NH)
Deleted: that
Deleted: contribute
Deleted: determining
Deleted: NH stratospheric
Deleted: by the enhanced aerosol layer
Deleted: a
Deleted: spatio-temporal surface temperature and land-sea thermal contrast
Deleted: an increase in atmospheric
Deleted:
Deleted: , leading to an increased
Formatted: English (US)
Deleted:) and a weakening of the polar vortex. The

Deleted: The identification of a deterministic response such as increased SSWs following HL volcanic eruptions calls for increased attention given the widespread surface cooling SSWs can initiate, influence societies throughout the continental NH. Also, the sensitivity of such events to eruption magnitude needs to be evaluated in terms of a possible source of increased seasonal predictability of NH regional climates.

Formatted: Font: 11 pt, Not Bold

1 Introduction

The enhancement of the stratospheric aerosol layer, which typically occurs following strong sulfur-rich explosive volcanic eruptions, is an important driver of natural climate variability by imposing short-lived yet possibly very strong radiative anomalies within the atmospheric column (Robock, 2000; Timmreck, 2012; Zanchettin, 2017). This direct radiative effect can alter both meridional surface and stratospheric temperature gradients that can, in turn, initiate further dynamical climate responses on seasonal to decadal time scales (Church et al., 2005; Gleckler et al., 2006; Stenchikov et al., 2009; Shindell et al., 2009; Otterå et al., 2010; Zanchettin et al., 2012; Swingedouw et al., 2015). Direct radiative and dynamical responses critically depend on the spatiotemporal characteristics of the enhanced stratospheric aerosol layer, which ultimately depends on the characteristics of the eruption, such as magnitude, timing and location (Stenchikov et al., 2009; Shindell et al., 2009; Zanchettin et al., 2012; Swingedouw et al., 2015). Spatiotemporal characteristics of volcanic aerosol from high-latitude (HL), Northern Hemisphere (NH) eruptions are typically very different when compared to tropical eruptions. Accordingly, several studies have shown that high-latitude NH eruptions typically initiate different climate responses compared to tropical eruptions (Meronen et al., 2012; Pausata et al., 2015; Guðlaugsdóttir et al., 2018; Zambri et al., 2019; Sjolte et al., 2021). Therefore, tropical eruptions cannot be considered close analogs of high-latitude NH eruptions, underlining the need for more studies on the latter to further quantify their potential climate impacts (Zanchettin et al., 2016). In this study we explore how stratospheric sulfate aerosol enhancements largely constrained in the NH extratropics affect hemispheric-scale atmospheric dynamics, with a focus on the stratospheric polar vortex and on temporal evolution of responses through three perturbed winters.

The winter stratospheric polar vortex is considered to play a deciding role in distinguishing between the response to low- and high-latitude NH enhancements of the stratospheric sulfate aerosol layer, where opposite responses are expected to emerge under the same mechanism: When the stratospheric sulfate aerosol layer is enhanced at low latitudes, e.g., following tropical volcanic eruptions, local warming by infrared absorption increases the meridional stratospheric temperature gradient that can lead to a stratospheric polar vortex strengthening due to a thermal wind response (e.g., Zanchettin et al., 2012; Bittner et al., 2016). Conversely, the local warming from aerosols constrained at higher latitudes decreases the meridional temperature gradient, promoting a

Deleted: Radiative forcing

Deleted: refs like above). ¶

Deleted:

Deleted: A major potential

Deleted: character

Deleted: tropical

Deleted:

Deleted: eruptions concerns

Deleted: winter

Deleted: polar vortex response.

Deleted: , or many others…).

Deleted: enabling

2

103 weakening of the polar vortex (Kodera, 1994; Perlwitz & Graf, 1995; Stenchikov et al., 2002;

104 Oman et al., 2005; Sjolte et al., 2021). The downward propagation of the stratospheric polar vortex

105 anomaly into the troposphere can lead to regime shifts of the tropospheric Arctic Oscillation and

106 associated anomalous regional surface patterns (e.g., Zanchettin et al., 2012; Zambri et al., 2017).

107 In the case of polar vortex weakening, a critical role is attributed to increased likelihood of sudden

108 stratospheric warming events (SSWs) (Haynes, 2005; Domeisen et al., 2020; Huang et al., 2021;

109 Kolstad et al., 2022, and references therein), whose projection on a negative Arctic Oscillation is

110 expected to bring a series of consequences, including increased frequency of tropospheric

111 blockings and mid-latitude cold air outbreaks (e.g., Ma et al., 2024). However, the negative Arctic

112 Oscillation and associated tropospheric anomalies following SSWs are characterized by a low

113 signal-to-noise ratio (e.g., Charlton-Perez et al. 2018; Zhang et al. 2019). Accordingly, recent

114 studies tend to disagree on this top-down mechanism being a robust dominant feature of climate

115 response to volcanic eruptions (Weierbach et al., 2023; DallaSanta and Polvani, 2023; Kolstad et

116 al., 2022; Azoulay et al., 2021; Polvani et al., 2019; Zanchettin et al., 2022; Toohey et al., 2014).

117 The radiative surface cooling following large volcanic eruptions has been shown to affect the

118 stratospheric polar vortex via a bottom-up mechanism (e.g., Graf et al., 2014; Peings and

119 Magnusdottir, 2015; Omrani et al., 2022). An example of this bottom-up mechanism following HL

120 eruptions is demonstrated in Sjolte et al. (2021) where they linked a weak polar vortex to an

121 increase in wave energy flux from the troposphere into the stratosphere without the meridional

122 stratospheric temperature gradient playing a major role.

123 With this in mind, the importance of transient atmospheric eddies (waves) and eddy-mean flow

124 interactions is becoming increasingly clear in explaining vertical and horizontal propagation of

125 atmospheric perturbations of various origins (e.g. Smith et al., 2022; Nakamura, 2023). DallaSanta

126 et al. (2019) used a hierarchy of simplified atmospheric models to show that eddy feedbacks are

127 crucial in explaining stratosphere-troposphere coupling as well as the stratospheric response alone

128 following a tropical Pinatubo-like eruption. This demonstrates that the anomalous atmospheric

129 circulation response to an enhanced stratospheric sulfate aerosol layer cannot be understood as

130 the mere adjustment to meridional temperature gradients, and that eddy-mean flow interactions

131 and eddy feedback are an essential contribution to such response. Both mechanisms, i.e., the top-

132 down mechanism triggered by local stratospheric heating and the bottom-up mechanism triggered

133 by surface cooling, act together in the real world and in realistic simulations. Therefore, idealized

Deleted: Bittner et al., 2016;

Deleted: ¶
¶
A strengthened

Deleted: can affect

Deleted: as the positive phase

Deleted: Northern Annular Mode), while a weaker

Deleted: linked

Deleted: in the stratosphere and a negative Northern Annular Mode in the lower troposphere

Deleted: demonstrating an example of a top-down mechanism. ¶
With its origin in the noisy stratosphere, this top-down mechanism can result in tropospheric signatures following volcanic eruptions. However, the signature tends to be weak in both observations and numerical simulations due to the different realizations and advanced statistical methods needed to extract the signal from the noise

Deleted: to

Deleted: interferences

Deleted: mediations

Deleted: stratospheric

Deleted: They also identified the extra-tropics as a dominant pathway in which the stratospheric response leads the troposphere following the eruption, a pathway similar to the response to SSWs. …

Deleted: following volcanic eruptions does not solely depend on simplified physics via

Deleted: where

Deleted: appear to be

Deleted: . Since both

Deleted: ,

Deleted: , under realistic volcanic forcing

3

167   model experiments are required to assess their relative contribution to uncertainty in regional
168   climate variability during the period following the enhancement of the sulfate aerosol layer
169   (Zanchettin et al., 2016).

170   In the definition of a framework to study the climatic effects of a high-latitude enhancement of the
171   stratospheric sulfate aerosol layer, Icelandic volcanism provides for an ideal test bed, as it has
172   played a role in shaping past NH climate variability and will continue doing so. Two Icelandic
173   eruptions during the past 2000 years, namely Eldgjá in ~939 CE and Laki in 1783 CE, are
174   considered to have had a significant impact on climate variability up to the global scale
175   (Brugnatelli and Tibaldi, 2020; Zambri et al., 2019; Oppenheimer et al., 2018; Thordarson and
176   Self, 2003; Stothers, 1998). These types of effusive eruptions are common in Iceland where their
177   duration can extend over years. During part of the eruption time such eruptions can become
178   explosive (referred to as mixed-phase eruptions) when ascending magma in a conduit comes in
179   contact with water as was considered the case with both Eldgjá and Laki, explaining their
180   widespread impacts. Eruption history as well as dense monitoring network of Icelandic volcanic
181   systems tell us that many of these systems are currently on the verge of an eruption, having already
182   produced some of the largest volcanic eruptions over the past millennia (e.g., Öræfajökull,
183   Bárðabunga and Hekla, Larsen & Guðmundsson, 2014; Barsotti et al., 2018; Einarsson, 2019).
184   Therefore history and current activity makes these types of eruptions an ideal reference case to
185   explore the potential climatic impacts of high-latitude enhancements of the stratospheric sulfate
186   aerosol layer and to test hypotheses about the underlying mechanisms driving the climate
187   response. This is the focal point of this study where we investigate for the first time the role of
188   wave-mean flow interactions and SSWs in the atmospheric circulation response to a HL volcanic
189   eruption. For this we perform idealized, long-lasting HL volcanic perturbation experiments using
190   the Community Earth System Model version 1 (CESM1) in its coupled and atmosphere-
191   standalone configurations. We evaluate the NH response during the first three winters following
192   the eruption, referred to as post-eruption winters in the text, and assess the dominating
193   mechanism in each winter. This paper is organized as follows: Section 2 describes the model,
194   experimental design and diagnostics; results are presented in section 3 followed by discussions in
195   section 4 where we end with concluding our results in section 5.

196

197

2 Methods

2.1. Numerical Model

We use the Community Earth System Model (CESM) version 1, developed by the National Center for Atmospheric Research (NCAR). In our configuration of CESM1, the atmospheric component is the Whole Atmosphere Community Climate Model, version 4 (WACCM4, Marsh et al. 2013). WACCM4 includes 66 vertical levels (up to $5.1\times10-6$ hPa, ~140 km) and uses CAM4 physics. We use the specified chemistry version of WACCM4 (SC-WACCM4), which is computationally less expensive to run, but simulates dynamical stratosphere-troposphere coupling and stratospheric variability like SSWs and the polar vortex with skills comparable to the interactive chemistry model version (Smith et al., 2014). CESM1/WACCM4 uses the Community Atmospheric Model Radiative Transfer (CAMRT) to parameterize the radiative forcing where it has been shown to accurately represent stratospheric aerosols by f. ex. simulating the temperature response following Mt. Pinatubo in 1991 (Neely et al., 2016). The SC-WACCM4 experiments are run with a horizontal resolution of 1.9° latitude by 2.5° longitude and include present-day (year 2000) radiative forcing. A repeating 28-month full cycle of the Quasi-biennial Oscillation (QBO) is included in the SC-WACCM4 experiments through nudging of the equatorial stratospheric winds to observed radiosonde data. In the coupled ocean-atmosphere configuration, the ocean component of CESM1 is the Parallel Ocean Program version 2 (POP2). CESM1 also includes the Los Alamos sea-ice model (CICE), the Community Land Model version 4 (CLM4) and the River Transport Model (RTM). CLM is run at a horizontal resolution of 1.9°x2.5°, POP2 and CICE are run at nominal 1° resolution with higher resolution near the equator than at the poles. Further details about CESM1 are given in Hurrell et al. (2013).

2.2. Volcanic Forcing File

We use the Easy Volcanic Aerosol (EVA) forcing generator (Toohey et al., 2016). EVA provides zonally symmetric stratospheric aerosol optical properties as a function of time, latitude, height, and wavelength (see detailed information on the tool in Toohey et al., 2016). EVA has been used to generate volcanic forcing in both idealized volcanic experiments (e.g., Zanchettin et al., 2016) and realistic paleoclimate simulations (Jungclaus et al., 2017) contributing to the sixth phase of the coupled model intercomparison project.

242 We use EVA to prescribe the volcanic aerosol loading corresponding to that of the 1991 Mt.
243 Pinatubo eruption (14.04 Tg SO_2), but at 45° N. Since the model reads the volcanic forcing as
244 aerosol mass (kg/kg), we scale our forcing file by using the standard aerosol mass input file for
245 CAM4 and 5 (see Neely et al., 2016, Table 1) for the same eruption. A monthly scaling factor was
246 derived from this linear relationship between the aerosol extinction ($1/m^2$) and the aerosol mass
247 (kg/kg) that was used to scale the raw EVA forcing data (Fig. 1). From these scaled forcing data,
248 the aerosol optical properties for our experiments are obtained with a two-step approach. First, we
249 move the injection location northwards so that the center of the aerosol mass is at 65° N latitude
250 and spans 10-28 km in altitude. Then, we define the start of the eruption to be May 1st and prolong
251 the peak of the forcing by extending in time the highest monthly value in the so-obtained forcing
252 data, so that the decline in aerosol mass begins 6 months after the start of the eruption or on
253 November 1 (see Fig. 1). We thus obtain aerosol optical properties for an idealized, long-lasting
254 high-latitude NH eruption. In this experiment we assume stratospheric injection only, although
255 similar eruptions in the natural world would likely inject part of the total aerosol mass within the
256 troposphere during the eruption. Past NH eruptions like Eldgjá and Laki had an atmospheric SO_2
257 loading of 219Tg and 122Tg respectively, that was carried aloft with the eruptive column up into
258 the upper troposphere with portions of the aerosols reaching the lower stratosphere during the
259 eruptions (Thordarson et al., 2001). Hence our experiment can also be considered as a 6-month
260 stratospheric aerosol injection that is analogous to similar although smaller eruptions (as compared
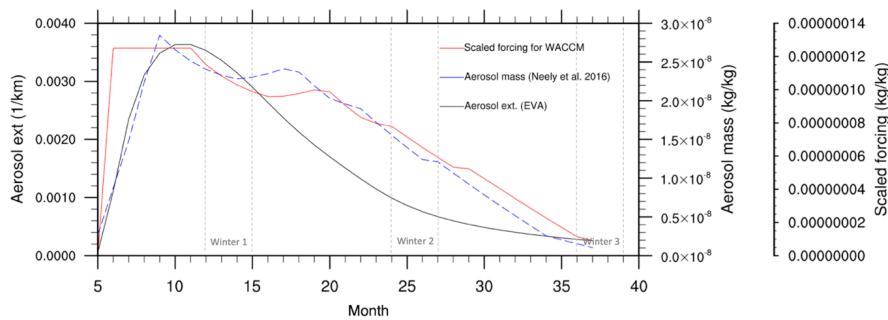261 to Laki) without the tropospheric aerosols.

262

263

264

265

Deleted: October

Deleted: Laki and

Deleted: 210Tg

Deleted: 120Tg

Deleted: , much larger than our 14Tg eruption,
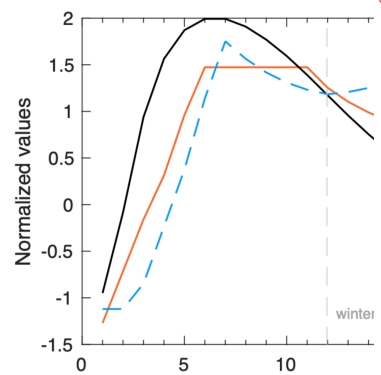
Deleted:

272   Figure 1: The time series of the original EVA aerosol extinction output (1/km, black curve) and the

273   aerosol mass of the volcanic forcing file of Neely et al. (2016) (kg/kg, blue dashed curve) used for

274   deriving the linear scaling coefficient for the conversion of EVA output into WACCM4 input

275   (kg/kg, red curve). The horizontal axis is time (months) from the start of the eruption. Here we

276   assume that the aerosol lifetime at 65° N is the same as at 45° N. Dashed vertical lines show the

277   three winters that we focus on in this study.

278

2.3. Experimental design

280   We ran two volcanic perturbation experiments with CESM1. The first experiment is conducted

281   with the atmosphere-only version of the model, where boundaries to SC-WACCM4 are provided

282   by prescribed fields of sea-surface temperature (SST) and sea-ice concentration (SIC)

283   corresponding to the 1979-2008 monthly climatology of HadISST observations (Rayner et al.,

284   2003). We refer to this experiment as *atm-only*. The second experiment is conducted with the

285   coupled version of the model, henceforth referred to as *cpl*. For each experiment we run 20

286   ensemble members including the volcanic forcing and 20 paired ensemble members without the

287   volcanic forcing and otherwise identical to the volcanic simulations, which we refer to as the

288   control.

289   The atmosphere-only experiments were run over three full years, which provides two full winters

290   after the onset of the eruption. We found that there was no need to extend the simulations further

291   given the duration of the forcing and short memory of the atmosphere. The coupled experiments

292   follow a similar protocol but they were integrated over 15 years to assess the response influenced

293   by oceanic dynamical adjustment. However, in this study we only focus on the first three winters

294   following the eruption. We define the first post-volcanic winter as December of the starting year

295   (year 0) and the following January and February (year 1), the second post-volcanic winter is then

296   December of year 1 and the following January and February of year 2 etc.

297   Because the QBO is prescribed, and given its importance for the atmospheric circulation and the

298   distribution of volcanic aerosols within the stratosphere (Thomas et al., 2009; DallaSanta et al.,

299   2021; Brown et al., 2023), we have been careful in homogeneously sampling the QBO phasing

300   that is imposed on the 20 ensemble members. For this, we shift the 28-month QBO cycle by one

301   month for every ensemble member, so that the phasing of the QBO differs from one ensemble

Formatted: Header

Deleted: The time series are normalized (mean=0, standard deviation=1) to allow comparison of time series with different units. …

Formatted: Font: Bold

Deleted: ¶

Deleted:

Deleted: to

308   member to the next (Elsbury et al., 2021). This avoids potential biases in the climatic response that
309   may be induced by any dominating QBO phase.
310
311   **2.4. Diagnostics**
312   Model output is analyzed by computing paired anomalies, defined as deviations of each volcanic
313   simulation from the corresponding control simulation (Zanchettin et al., 2022) (volcanic minus
314   control). The statistical significance of the ensemble mean of paired anomalies is assessed at the
315   95% confidence interval, calculated from all 20 ensemble members, using a two-sided Student's t-
316   test in addition to a Kolmogorov-Smirnov test.
317   To evaluate the effects of planetary waves on the zonally-averaged stratospheric response, we use
318   the Eliassen Palm (EP) flux and its divergence (Edmon et al., 1980) in addition to the 3D
319   generalization of the EP flux, the Plumb flux (Plumb, 1985), for a longitudinal representation in
320   the lower troposphere and stratosphere. We identify SSW events by using an algorithm following
321   the procedures described in Charlton and Polvani (2007), where mid-winter sudden warming
322   events are determined to take place if the 10 hPa zonal-mean zonal wind at 60°N becomes easterly.
323   Once a warming is identified, no day within 20 days of a central date, defined as the first day in
324   which the daily mean zonal-mean wind at 60N and 10hPa is easterly, can be defined as an SSW.
325   Changes in conditions for large-scale planetary waves propagation (waveguides) are examined
326   using the optimal propagation diagnostic for stationary planetary waves, described in Karami et
327   al. (2016). This metric is based on the construction of PDFs for positive values of the refractive
328   index (Matsuno 1970), as a function of zonal and meridional wave numbers. The refractive index
329   is calculated using daily zonal wind and temperature at all levels, to derive monthly and zonally-
330   averaged probabilities for stationary Rossby waves to propagate through the atmosphere, in
331   function of latitude and pressure level. This is calculated for zonal wave numbers k=1,2,3 and
332   meridional wave numbers l=1,2,3 (large-scale waves), and we average the probabilistic refractive
333   index for each of the nine combinations of k and l, to provide a general estimate of chances for
334   propagation of stationary planetary waves. For the eddy feedback calculations we compute the
335   square of the local correlation across the ensemble members between DJF zonal-mean zonal wind
336   and the divergence of the northward EP flux (delta phi F phi) averaged over 600-200 hPa (Smith
337   et al. 2022). In addition, we compute the rate of temperature (K) changes in the 2m temperature

Deleted: student's

Deleted:

Deleted: mean wind at 60N and 10hPa is easterly, can be defined as an SSW.

Deleted:

8

343 (T2m) gradient using spherical harmonics to yield a T2m gradient in the meridional (dZ/dlat) and
344 zonal (dZ/dlon) directions.

345

346 **3 Results**

347 In the following sections we will investigate the *cpl* experiment to characterize the forced response
348 and identify the mechanism by utilizing the information provided by the *atm-only* experiment. We
349 begin our investigation in the upper atmosphere before making our way towards the surface.

350

351 **3.1. Volcanic radiative forcing**

352 The net shortwave (SW) and longwave (LW) downward flux at the top of the atmosphere show an
353 expected behavior following a stratospheric sulfate injection where we see a decrease in the SW
354 due to scattering and an increase in the LW due to absorption around the injection location (Fig.
355 2c-f). Temporal perturbations of SW fluxes for both *cpl* and *atm-only* are influenced by the obvious
356 strong seasonal evolution in solar insolation, where we see strong anomalies during the first
357 summer north of 30° N than then becomes more confined to the mid latitudes as winter progresses
358 with a slow decrease towards the end of the third year (Fig. 2c-d).
359 LW anomalies also show seasonal evolution with stronger LW flux at mid latitudes compared to
360 at high latitudes during summer that continues into the winter season and remains significant
361 throughout most of these three years. During winter, the LW anomalies are present at high latitudes
362 where the SW anomalies are absent. The latitudinal bands of radiative flux anomalies correspond
363 to the maximum values of the aerosol mass between 60 and 70° N, and the aerosol mass being
364 largely confined north of 45° N (Fig. 2a-b). Overall, the radiative forcing is largely bounded by
365 the NH extratropics with the exception of a slight significant increase around 30-60° S in the
366 second and third summer (Fig. 2c-d) that is visible at around 14-15 km a.s. (Fig. 2b). This occurs
367 due to spatial features in the Neely et al. (2016) aerosol forcing that we use for scaling, where a
368 slight aerosol increase occurs at lower latitudes, although this is not detectable when the aerosol
369 mass is averaged through the atmospheric column with respect to time (Fig. 2a). We also detect a
370 slight difference in the LW and SW fluxes that arises from differences in high cloud cover between
371 *atm-only* and *cpl*, where *cpl* shows a decrease in high cloud cover in the northern high-latitudes,
372 compared to *atm-only* (not shown).

373
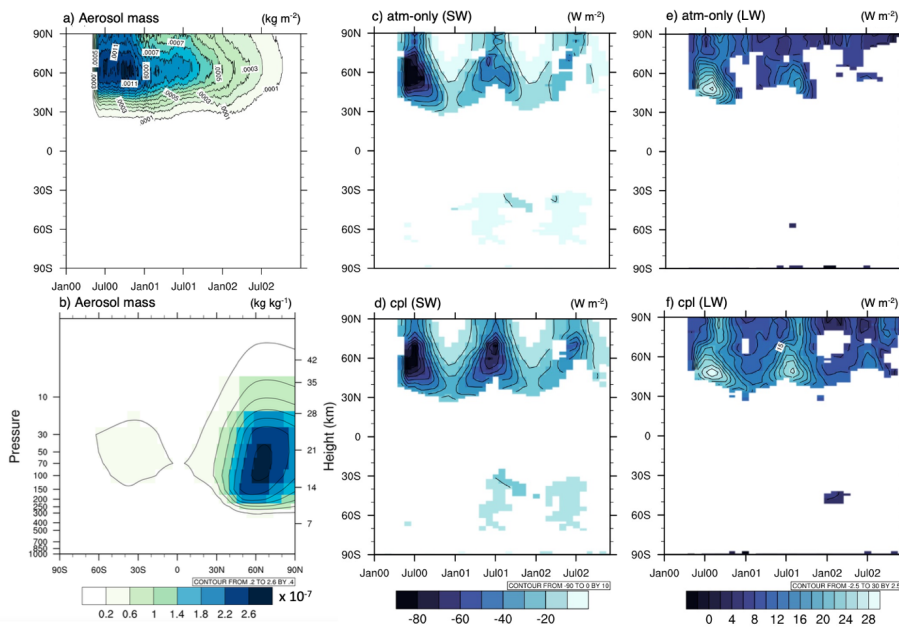
Figure 2: Left panels: a) Average aerosol column mass time evolution in kg/m2 and b) pressure vs. latitude slice of the aerosol mass in kg/kg (3-year average). Aerosol mass is the same in cpl and atm-only. c) and d) show the time evolution of the net SW flux (downward) anomaly at the top of the atmosphere, and e) and f) the same but for net LW flux anomaly, resulting from the volcanic aerosol mass, in c) *atm-only* and d) *cpl* where coloured areas indicate 99% significance compared to the control experiment according to a Student's t-test.

3.2. Stratospheric response

The strong seasonality in the LW perturbations described above also characterizes stratospheric temperatures, where a strong increase in the zonally averaged temperature at 50 hPa (T50) is detected north of 30° N during post-eruption summers in both experiments (Fig. 3a and 3b). This summer warming is followed by a net cooling of the polar stratosphere in the first winter seen for both *cpl* and *atm-only*. A clear difference in the T50 response in the two experiments is seen in

10
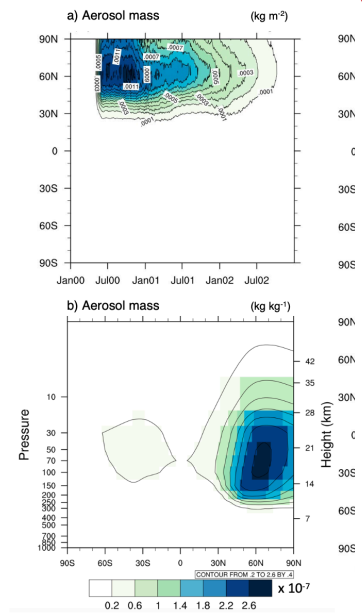
398 winter 2, where *cpl* yields warming over polar latitudes while *atm-only* yields cooling (Fig. 3a,b).

399 This reveals the intra-seasonal dynamical effects in the *cpl* experiment beyond the direct radiative

400 response as we will see later on. The contrasting temperature response is accompanied by an

401 opposite response in the zonal-mean zonal winds at 10hPa (U10) between 70 and 80° N. This U10

402 response is an indicator of the state of the polar vortex, where a polar vortex weakening is detected

403 in winter 2 for *cpl* but a strengthening *atm-only* (Fig. 3c-d). Figures 3c-d do show a large ensemble

404 spread in the zonal mean U10 winter response that is evident of a low signal to noise ratio. While

405 the first winter in *cpl* and the first two in *atm-only* show little statistical significance according to

406 a Kolmogorov-Smirnov test, this significance does increase for winter 2 in the *cpl* experiment. We

407 also see this weakening in the zonal mean U50, also showing stronger significance during winter,

408 (Supplementary Fig. S3) but not as clearly as in the zonal mean U10. However, for consistency we

409 will mainly be focusing on the U50 response in the following section where this response is clear

410 over the NH polar cap. The difference between *cpl* and *atm-only* will be in the focus in the
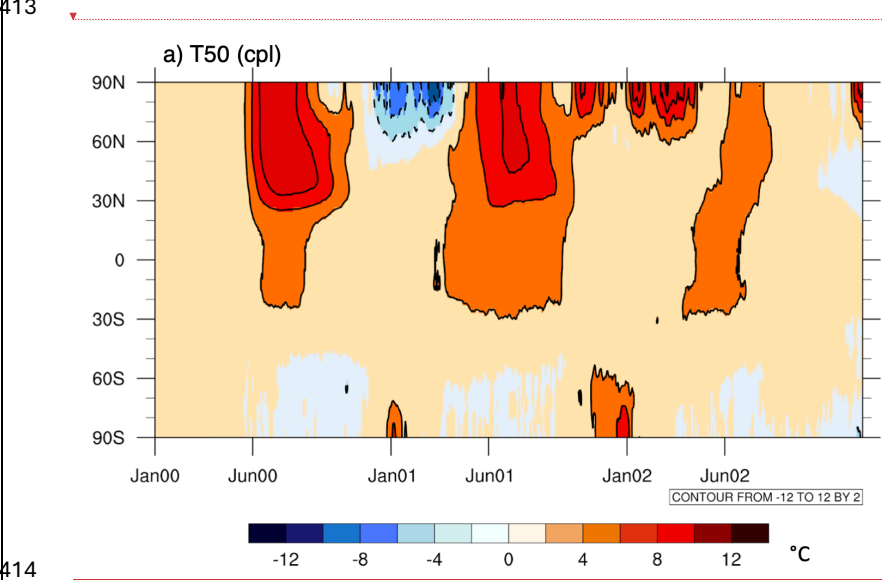
411 following sections.

412

413

a) T50 (cpl)

CONTOUR FROM -12 TO 12 BY 2

414

b) T50 (atm-only)

420

c) U10 (cpl)   d) U10 (atm-only)

421
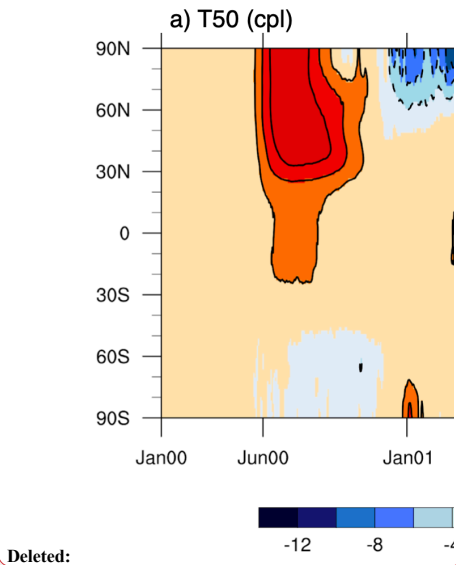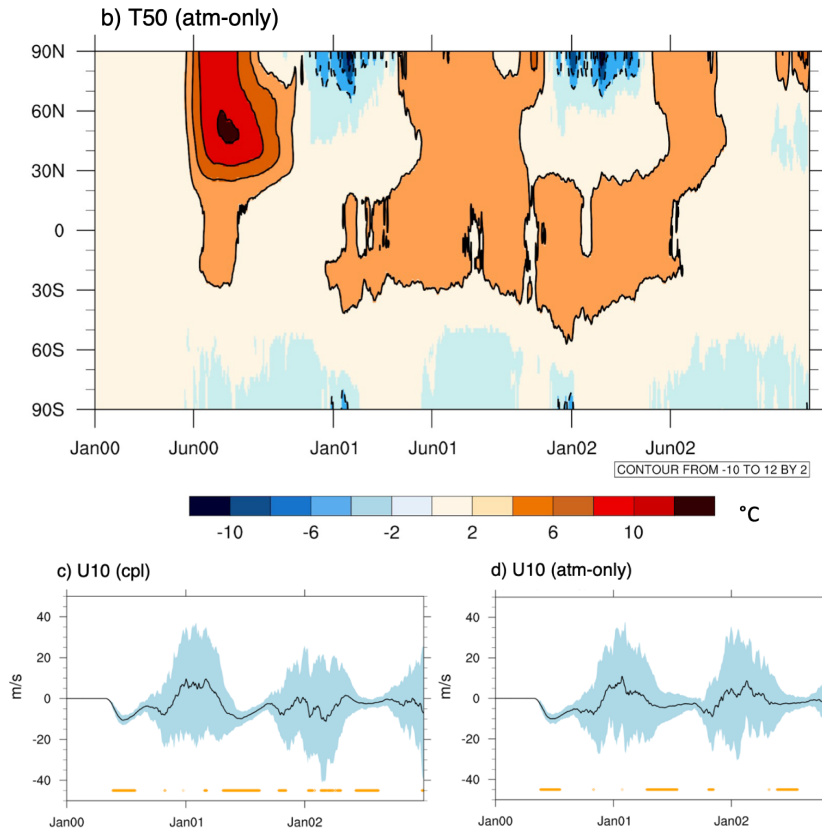
Figure 3. a,b) Latitude versus time response of T50 anomalies in a) *cpl* and b) *atm-only*. Contours are significant in 95% confidence intervals according to a student's t-test. c,d) Stratospheric polar vortex response shown as the zonal mean U10 anomalies between 70 and 80° N for c) *cpl* and d) *atm-only*. Black lines show the ensemble mean anomalies and blue shadings show the ensemble +/- 2 standard deviation anomaly range. Orange markers indicate when the difference between perturbed and unperturbed experiments becomes significant (p<0.05) according to a Kolmogorov-Smirnov test.

429

430

431

3.2.1 - First post-eruption winter

In the *cpl* experiment, the polar vortex strengthening in winter 1 is associated with extensive anomalies in temperature and zonal wind at 50 hPa (Fig. 4a). The anomalous temperature pattern consists of cooling at high latitudes and into the midlatitudes over the Atlantic, and warming over large swaths of the subtropics (to 20° N) and into the midlatitudes over the Pacific. This temperature pattern is also identified in the zonal mean T50 (Fig. 3b). Similarly, the zonal wind weakens into the midlatitudes over the Pacific while it is stronger in mid to high latitudes over the Atlantic. The strong upward EP flux (black arrows) is an indicator of the direction of propagated waves originating at the surface around the midlatitudes, where the horizontal and vertical EP flux components are proportional to the eddy momentum and heat flux, respectively (Fig. 4d). A convergence (negative divergence, dashed red contours) in the EP flux is detected in the upper troposphere that acts to weaken the tropospheric westerlies (Fig. 4d and Fig. S2). However, the EP flux and its convergence within the stratosphere does not appear to impact the stratospheric mean flow and the polar vortex. Therefore, the local heating due to the volcanic aerosols and the associated increase in the meridional temperature gradient in the stratosphere appear to dominate the response of the polar vortex via thermal wind response, also depicted by the LW anomalies (Fig. 2f). Winter 1 in *atm-only* shows a similar thermal wind mechanism at play in the stratosphere as for the *cpl* experiment (Fig. 5a and 4a, respectively). In that case, less obvious tropospheric influences are detected, due to lack of forced surface cooling, as seen in the limited anomalous upward wave activity detected by the EP flux diagnostics (Fig. 5c).

13
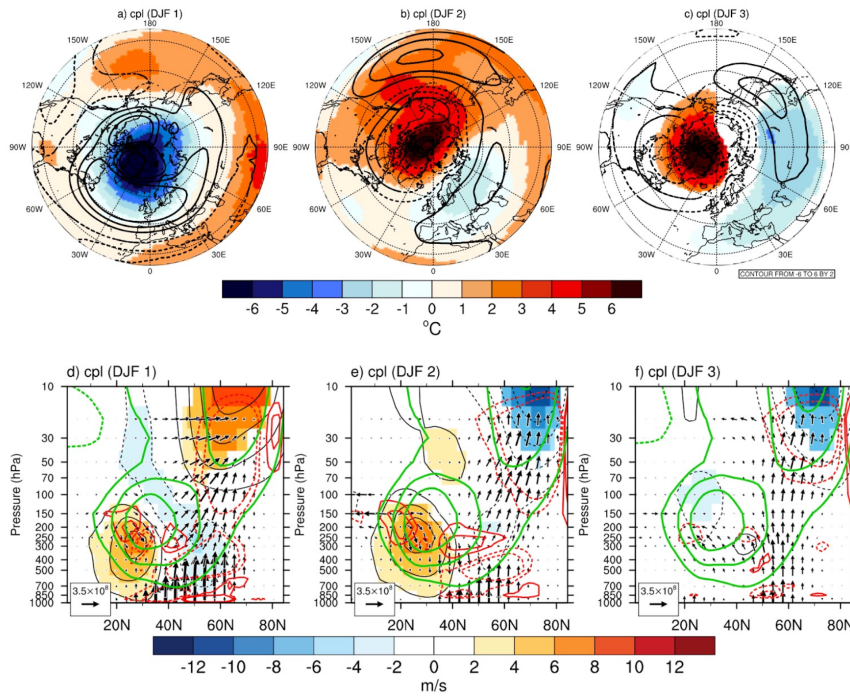
Figure 4: Winter stratospheric response in the *cpl* experiment. a-c) U50 (contours) and T50 (shading: red = warming, blue = cooling) response for winters 1-3, respectively. d-f) EP flux (arrows) and divergence (red contours) response, along with zonal-mean zonal wind response (black contours and shading: red = strengthening, blue = weakening) and climatology (green contours) in winters 1-3, respectively. Contours and color-shaded areas indicate 95% significance according to a Student's t-test. Only vectors that are significant at the 95% confidence interval are shown.

482
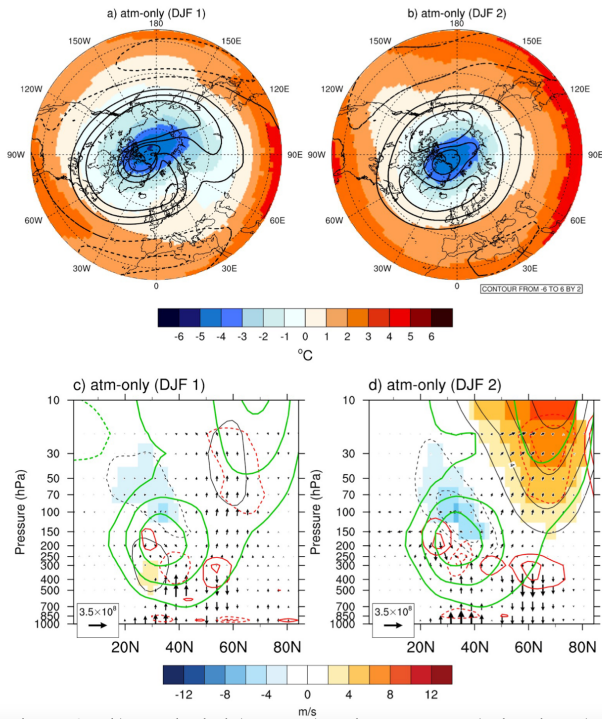
Figure 5: The same as Fig. 4 but for the *atm-only* experiment. a-b) Zonal wind (contours) and
temperature (shading) response at 50 hPa for winter 1 and winter 2, respectively. c-d) EP flux
(arrows) and divergence (red contours) response along with zonal-mean zonal wind (black
contours) and pure climatology (green contours, 2m) in winters 1-2, respectively. Contours and
colored area indicate 95% significance according to a Student's t-test.

3.2.2. Second post-eruption winter

A stark difference in the polar vortex response is detected between *cpl* and *atm-only* in winter 2.
While *atm-only* exhibits a response similar to winter 1 (Fig. 5b), a significant warming over North
America and the North Pacific emerges in *cpl* along with a weakening of U50 at high latitudes
(Fig. 4b) indicating a shift of the polar vortex towards Eurasia. This warming at high latitudes then
coincides with a slight LW absorption at high latitudes (Fig. 2f). The U50 weakening is not uniform
throughout the longitudes explaining the lack of response detected in the zonal mean U50 (Fig.

15

Deleted: student's

Formatted: Font: Italic

Deleted: Supplementary

498 S3), where one needs to go to U10 to get a clear response in the zonal-mean zonal wind (Fig. 3c).

499 An anomalously strong upward propagation of planetary waves persists in the *cpl* (Fig. 4e), with

500 a stronger upward EP flux now protruding into the stratosphere above 20hPa in contrast to winter

501 1. The upward EP flux and its convergence in the polar stratosphere are evident of their

502 contribution towards the weakening of the U50 and a general dominance over the effects of thermal

503 forcing by aerosols that have been, at this stage, substantially reduced (Fig. 1).

504 Similar wave propagation pattern as identified in the *cpl* experiment is known to be associated

505 with SSWs. We suspect that the decrease in the T50 difference between mid- and high latitudes

506 can act as a trigger for a weaker polar vortex in addition to the stratosphere absorbing the upward

507 propagating waves that is known to cause warming over the polar cap (Kodera et al., 2016;

508 Kretschmer et al., 2018). We will see further evidence of this in the next section.

509

510 **3.2.3. Third post-eruption winter**

511 The results in this section only refer to the *cpl* experiment since winter 3 is lacking in *atm-only*.

512 The SSW-like pattern of winter 2 clearly continues into winter 3, where most of the volcanic

513 aerosols have decreased to the extent that their radiative impacts no longer dominate. An exception

514 is the confinement of T50 warming over the polar stratosphere (Fig. 4c). Furthermore, anomalous

515 upward propagation of planetary waves continues to persist (Fig. 4f). This upward wave flux in

516 addition to the T50 warming resembles a pattern that behaves much like absorbing SSWs defined

517 by Kodera et al. (2016). To examine this response further we define SSWs based on the reversal

518 of the zonal-mean zonal winds at 60° N and at 10hPa between November and March according to

519 the method of Charlton and Polvani (2007) .

520

521 Results from the SSW analysis are presented in Fig. 6. No significant increase in SSWs is found

522 in winter 2, despite the SSW-like pattern detected. This changes in winter 3 when the difference

523 between perturbed and unperturbed experiment becomes statistically significant, with 27 SSWs

524 occurring in our forced experiment compared to only 6 in the control experiment. This increase in

525 SSWs agrees well with the U50 and T50 anomalies of winter 3 (Fig. 4c). During winter 2, the

526 warming of the polar stratosphere is as strong as in winter 3 but more spread out into midlatitudes.

527 These results are also in agreement with the stratospheric Plumb flux in winter 3 (Fig. S1c) where

Deleted: above 50hPa,

Deleted: ,

Deleted:

Deleted: reflection

Deleted: , where we

Deleted: and the pole

Deleted: , except that

Deleted: is now confined

Deleted: Anomalous

Deleted:

Deleted: (p-value = 2.6e-4).

Deleted: Although the response in winter 2 does not lead to as many SSWs despite the weaker zonal winds, it does appear to act as an important precursor to the significant increase in SSWs detected in winter 3.

Deleted: Supplementary

16

544 the upward flux is mostly circumpolar between 40° and 60° N, showing further evidence of the
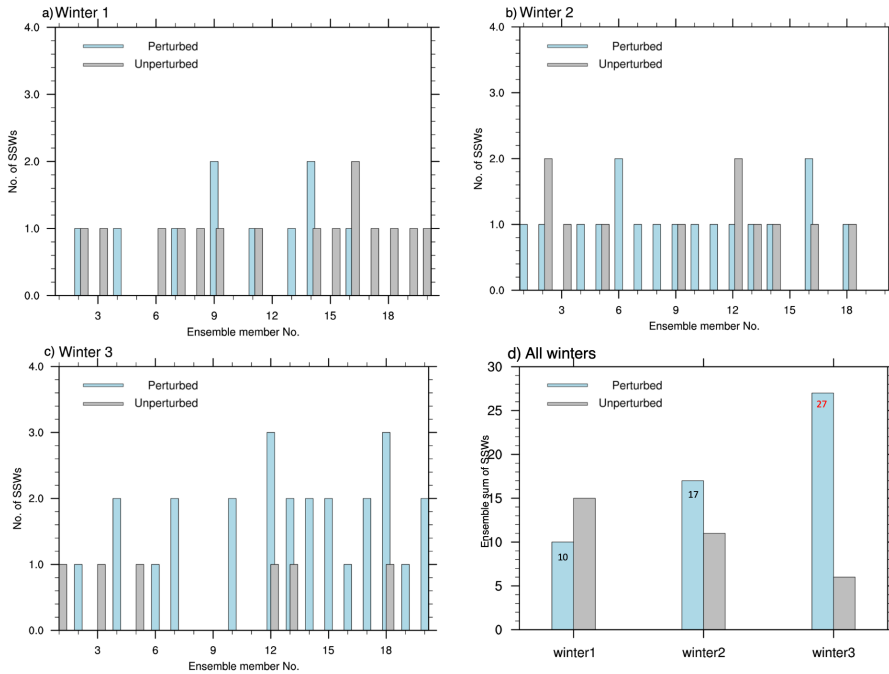
545 SSWs detected.

546

547

548 Figure 6: a-c) The number of SSWs during winters 1-3 for each ensemble member in the *cpl*

549 experiment and d) The sum of all SSWs in each experiment for all 20 ensemble members of winters

550 1-3 both for *cpl* (light-blue bars) and control (gray bars). The color red indicates 95% significance

551 according to a two-sided Student's t test.

552

553 When comparing the ensemble sum of SSWs in the perturbed and unperturbed experiment using

554 a Kolmogorov-Smirnov test (Fig. 5d), a significant increase in the number of SSWs occurs in

555 winter 3 (p=0.0135). This underlines the generally strong SSW response occurring in winter 3,

556 when the fraction of ensemble members having more than 1 SSW per winter increases to 50% (10

557 ensemble members) in winter 3 compared to only 10% in winters 1-2. Of these 10 ensemble

558 members, two members show three SSWs per winter that can be considered highly unlikely based

17

561 on historical records. Although winters with more than 1 SSWs are considered unusual, examples

562 do exist in the observational record of multiple SSWs in one winter, like the winter of 1998/1999

563 and 2009/2010 (Kodera et al., 2016 and Ineson et al., 2023 respectively).

564 To better understand the cpl SSWs response, we also did an SSW analysis on *atm-only* (Fig. S7)

565 where 50-75% less SSWs were detected in the perturbed simulation compared to the unperturbed

566 one. Such a response should not be unexpected during the forced polar vortex strengthening as

567 detected in *atm-only* (see Fig. 5). Furthermore, only single SSWs per winter were detected in all

568 20 ensemble members of the perturbed simulation while two (one) ensemble member(s) detected

569 double SSWs per winter 1 (winter 2) in the unperturbed simulation. Although these results do show

570 strong evidence of an increase in the number of SSWs in the *cpl* simulation, internal variability is

571 large and the frequency of SSWs fluctuates substantially between the three winters in the

572 unperturbed simulation.

573 Since this is indicative of a low signal-to-noise ratio and uncertainties in the response of polar

574 vortex variability, we tested the potential impact of ensemble size on the signal-to-noise ratio for

575 two key diagnostics of our mechanism, namely U10 and SSW. We express the signal-to-noise ratio

576 as the uncertainty related to the expected (i.e., ensemble mean) response, calculated as standard

577 error of the mean of post-eruption paired anomalies for the first three post-eruption winters. The

578 standard errors converge toward the value obtained for the full 20-member ensemble for all winters

579 and both variables (Figure 7), with a common tendency of growing uncertainty in the expected

580 response with the ensemble size. The mean curves consistently level off for ensemble sizes larger

581 than 10, suggesting that the full ensemble estimate is representative of uncertainty in the expected

582 response for larger ensemble sizes. Otherwise, winter 3 produces larger uncertainty than winters 1

583 and 2, suggesting a less constrained forced response. This is especially evident for estimates of

584 standard error of SSW anomalies and ensemble sizes larger than 15, where winters 1 and 2 closely

585 superpose on each other while winter 3 does not overlap with winters 1 and 2 within the 5-95th

586 percentile range. Overall, the flattening of the ensemble-mean expectations on the standard error,

587 and the large values diagnosed in winter 3, suggest that the winter 3 response features an

588 intrinsically lower signal-to-noise ratio. In fact, since the value of full-ensemble mean SSW paired

589 anomaly in winter 3 (+1.05 events) is similar to the associated expected standard error (+1.02

590 events) we conclude that even a much larger ensemble would not provide more certainty in the

591 signal detected.
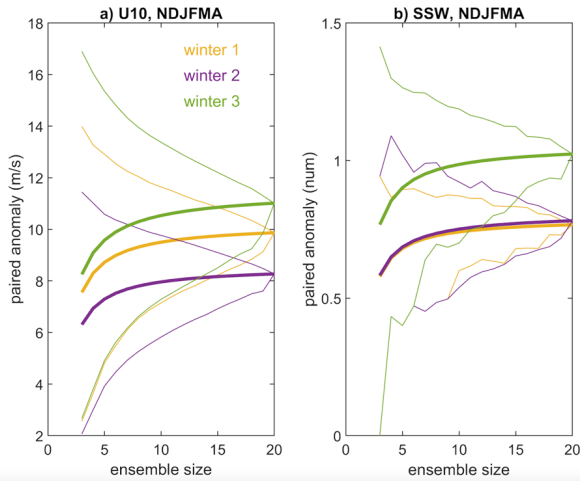
Figure 7: Impacts of ensemble size and spread on the volcanic signal. Ensemble mean (thick lines) and associated standard errors (thin lines, 5-95 percentile range) of paired anomalies calculated for different ensemble sizes and for the first three post-eruption extended winter seasons (November to April) for stratospheric zonal-mean zonal wind (a) and number of sudden stratospheric warming events (b). For each ensemble size from 3 to 20, the mean and the standard error of the mean are calculated for all sub-ensembles determined by all possible permutations of the full ensemble for the considered size. Then, means and 5th and 95th percentiles of the so-obtained standard errors for each ensemble size are plotted.

According to the above, the evolution in *cpl* from winter 1 to winter 3 can be summarized as follows: In the first winter, the thermal forcing appears to be stronger than the upward wave flux because of the large amount of aerosols present, thereby dominating the response that causes the polar vortex strengthening and the inclusion of cold polar air within. In the second winter, the thermal forcing from the volcanic aerosols at midlatitudes has decreased where it is now mostly confined to higher latitudes as seen both in the LW flux and T50 (Fig. 2f and Fig. 3b). We suspect that in addition to the aerosol decrease, this slight decrease in the temperature difference between high and midlatitudes allows the strong upward wave flux to dominate and enter the upper stratosphere. There in the stratosphere, the waves are absorbed that causes further warming over the polar cap in addition to weakening the zonal stratospheric winds (Fig. 5b and Fig. 4b). This

19

upward wave flux and weaker winds continue into the third winter, where winter 2 likely acts as a precursor, allowing for SSWs to develop more frequently as detected in the T50 warming that is now confined over the polar cap (Fig. 4c and Fig. 5c, respectively). The expected absence of a surface response is obvious in our *atm-only* experiment where basic physical mechanism, via the thermal wind balance due to radiative heating, dominates the atmospheric circulation response in the first two post-eruption winters, with a strong stratospheric polar vortex isolating the cold air over the polar regions in the second winter as in the *cpl* experiment (Fig. 5a-b).

3.3. Tropospheric response

What is it then that drives this polar vortex weakening and the SSW response in the *cpl* experiment? To examine in more detail the origin of the upward wave fluxes in winters 2 and 3 of the *cpl* experiment that causes the detected polar vortex weakening and the SSWs, we now turn our attention towards the troposphere.

We begin by comparing the response of T2m, vertical Plumb flux at 850 hPa and 200 hPa zonal wind, in *cpl* (Fig. 8) and in *atm-only* (Fig. 9). As a response to the decrease in SW flux following the eruption, extensive and heterogeneous cooling is identified in the T2m anomalies in winters 1-3 (*1-2 for atm-only*) over latitude bands that contain the most significant SW flux decrease (Fig. 2d, Fig. 8a-c and Fig. 9a-b). The strongest cooling occurs over northeastern North America and along the Asian midlatitudes in winter 1, with much larger amplitude in *cpl* than in *atm-only* (Fig. 8a versus Fig. 9a). In *cpl*, the SST significantly cools down (Fig. S5), which extends the area of negative T2m anomalies over the ocean, in particular over the northwestern North Pacific in winter 1 (Fig. 8a). There it progresses from an initial preferential surface cooling over the midlatitudes in winter 1 to a later cooling of polar regions in winter 3 (Fig. 8c). In *atm-only*, the surface response is hampered over the ocean by the experimental design, and T2m anomalies are therefore confined to landmasses, yielding an overall much weaker temperature response compared to *cpl* (Fig. 9a-b).
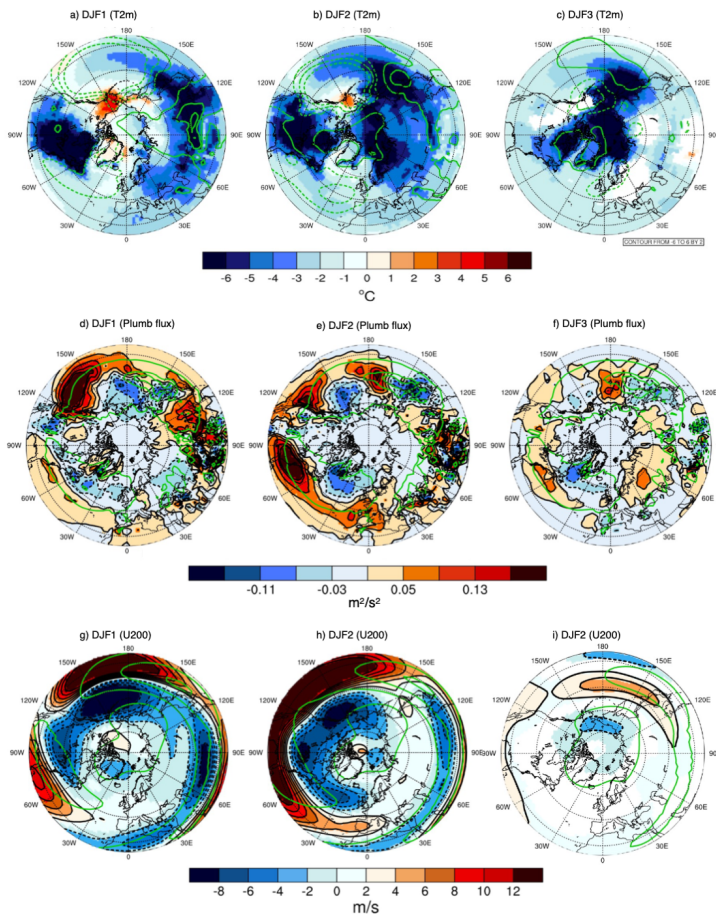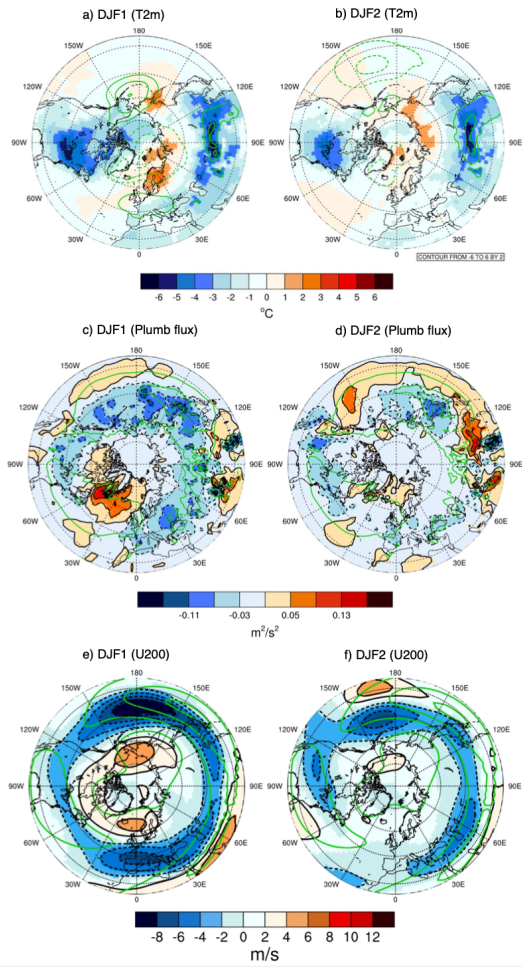
775

Figure 8. a) Response of 2-meter air temperature (°C) in *cpl* (color), and sea-level pressure (green

contours), for winter 1. b) Same as *a)* but for winter 2. c) Same as *a)* but for winter 3. d) Response

of 850 hPa vertical component of the Plumb flux (m²/s²) in *cpl*, and the climatology as green

contours from -8 to 12 by 2, for winter 1. e) Same as *d)* but for winter 2. f) Same as *d)* but for

winter 3. g) Response of 200 hPa zonal wind (m/s) in *cpl*, and the climatology as green contours

from -0.15 to 0.15 by 0.04, for winter 1. h) Same as *g)* but for winter 2. i) Same as *g)* but for winter

3. Contours and colored areas indicate significance at the 95% confidence interval according to a

Student's t-test.

21

789

a) DJF1 (T2m) b) DJF2 (T2m)

CONTOUR FROM -6 TO 6 BY 2

-6 -5 -4 -3 -2 -1 0 1 2 3 4 5 6
°C

c) DJF1 (Plumb flux) d) DJF2 (Plumb flux)

-0.11 -0.03 0.05 0.13
m²/s²

e) DJF1 (U200) f) DJF2 (U200)

-8 -6 -4 -2 0 2 4 6 8 10 12
m/s

790

Figure 9. a) Response of 2-meter air temperature (°C) in *atm-only,* and sea-level pressure (green contours), for winter 1. b) Same as *a)* but for winter 2. c) Response of 850 hPa vertical component of the Plumb flux (m²/s²) in *atm-only*, and the climatology as green contours from -8 to 12 by 2, for winter 1. d) Same as *c)* but for winter 2. e) Response of 200 hPa zonal wind (m/s) in *atm-only*, and the climatology as green contours from -0.15 to 0.15 by 0.04, for winter 1. f) Same as *e)* but

22

797 for winter 2. Contours and shaded areas indicate significance at the 95% confidence interval

798 according to a Student's t-test.

799

800 Figure 10. Probability (%) of favorable propagation conditions for large-scale stationary Rossby

801 waves (zonal and meridional wavenumbers 1, 2 and 3) as a function of latitude and pressure levels

802 (shading). Contours show the response in long_summer versus control. a) Winter 1 in *cpl*. b)

803 Winter 2 in *cpl*. c) Winter 3 in *cpl*. d) Winter 1 in *atm-only*. e) Winter 2 in *atm-only*.

804

805 The vertical component of the the Plumb flux at 850 hPa (Fig. 8d-f) allows us to locate the origins

806 of the upward EP flux in *cpl* (Fig. 4d-f). It is strongest over the north eastern part of the Pacific

807 Ocean (off the west coast of North America) in winter 1, where it continues up into the lower

808 stratosphere at 150 hPa (see Fig. S1a). In winter 2, the Plumb flux has decreased in the North

809 Pacific and increased over the North Atlantic and Siberia, pointing to a possible influence of the

810 change in land-sea temperature contrast (Fig. 8e). In addition to this upward flux, we also detect

811 downward wave flux over both the Aleutian and Greenland regions at 850 hPa and over a large

812 area south of 45° N at 150 hPa. This downward Plumb flux is evidence of changes in the planetary

Deleted: 3D wave activity flux (

Deleted:)

Deleted: 7d

Deleted: *cpl*

Deleted:) as being

Deleted: Supplementary

Deleted: vertical

Deleted: decreases

Deleted: increases

Deleted: 7e

Deleted: propagating

23

824 wave structure where wave reflection occurs due to the sudden weakening of the zonal winds
825 identified in the U10 (Fig. 3a). In winter 3, the Plumb flux now dominates both at 850 (seen in Fig.
826 8f) and 150 hPa (Fig. S1c), where it encircles the polar stratosphere north of 60° N. In line with
827 the weak EP-flux response shown in Fig. 5, the Plumb flux anomalies are generally weak in *atm-*
828 *only* compared to *cpl*, for both winter 1 and 2 (Fig. 9c-d).

829

830 Since upward wave activity depends on wave-mean flow interactions, several factors are at play
831 to explain the strong response in *cpl* vs *atm-only*. First, the change in zonal flow is substantially
832 different between the two pairs of experiments, as shown by the U200 anomalies (Fig. 8g-i and
833 Fig. 9e-f). In the first two winters we observe an intense deepening of the Aleutian low in *cpl* (Fig.
834 8a-b) associated with a large equatorward shift of the subtropical jet over the North Pacific (Fig.
835 8g-h, also seen in the zonal-mean averages of Fig. 4). The change in zonal flow is not as large in
836 *atm-only*, where there is a general decrease of U200 on the poleward side of the subtropical jets,
837 rather than a marked equatorward shift as in *cpl*. This further emphasizes that amplified surface
838 coupling when the ocean is coupled to the atmosphere has a dramatic impact on the amplitude of
839 the tropospheric response. Because the zonal flow acts as a waveguide for large-scale planetary
840 waves, we expect changes in upward wave propagation in the stratosphere. To measure how
841 waveguides change, Fig. 10 shows the probability of favorable propagation conditions for large-
842 scale stationary waves, averaged for zonal wave numbers k=1,2,3 and meridional wave numbers
843 l=1,2,3, as a function of pressure and latitude (see section 2 for more details). Areas of high
844 probability show where large-scale waves preferentially propagate, while low probability regions
845 indicate where linear wave propagation is hampered. Generally, the mid-latitude troposphere is
846 more favorable for wave propagation than the high-latitudes and the stratosphere, consistent with
847 the tendency for stationary waves to propagate upwards and to be deflected towards the equator,
848 in climatology. After injection of the volcanic forcing, both *cpl* and *atm-only* exhibit an increase
849 in the probability for wave propagation between 40 and 60 °N in the lower stratosphere during
850 winter 1 and 2, but the responses in the troposphere are markedly different. In *atm-only*, wave
851 propagation is inhibited in the free troposphere north of 60°N, for both winters 1 and 2 (Fig. 10d-
852 e), which is consistent with the EP-flux anomalies of Fig. 5. This response is absent from *cpl* during
853 winter 1 (Fig. 10a), and opposite during winter 2 when an increase of favorable conditions for
854 wave propagation is diagnosed (Fig. 10b). We also see that the waveguide has greatly reduced in

the subtropical troposphere in *cpl* winters 1-2 that favor large-scale waves to be redirected towards the pole. This increase in favorable conditions for wave propagation in the troposphere between 60 and 80 °N persists during winter 3 in *cpl* (Fig. 10c), which is a partial and the most likely explanation for enhanced upward wave propagation in the stratosphere described in Fig. 4f.

In *cpl* winter 3, when the cooling is reduced in the NH mid-latitudes and has migrated towards the polar regions, which is also evident in the SST (Fig. 5S), the amplitude of the 850 hPa upward Plumb flux anomalies decreases compared to previous winters (Fig. 8f). This suggests that the mid-latitude spatiotemporal cooling pattern plays a part in the strong wave activity detected near the surface. This can be revealed by computing the T2m gradient (Tgrad) where strong land-sea temperature gradients are known for their ability to influence atmospheric wave activity (Hoskins and Valdes, 1990; Brayshaw et al., 2009; He et al., 2014; Wake et al., 2014; Portal et al., 2022). In winter 1 the meridional gradient shows sharp significant changes encircling 45° N (Fig. 11a), with positive (negative) gradient anomalies occurring south (north) of 45° N. In winter 2 we still see the gradient present at 45° N but now located over North America and the North Pacific. Winter 3 mostly reveals regional anomalies in the Barents-Kara, Greenland-Iceland and the North Pacific regions (Figure 11b-c), occurring over areas of significant sea ice increase (not shown). A sharp Tgrad change throughout the NH at 45° N is identified in winter 1 (Fig. 11a) that is followed by a reduction of land-sea temperature contrast over eastern Canada and the U.S. in winter 2 (Fig. 11b). This is a known cause of planetary wave enhancement (Portal et al., 2022) and could provide an explanation for the strong surface upward wave flux detected in the second and third post-volcanic winters (Figure 8e-f). Both the zonal and meridional Tgrad components show an increase in the northern part of Alaska that coincides with the region of T2m warming over the Aleutian/Alaska region (Fig. 8a) and the strong upward Plumb flux (Fig. 8d). This warming, in addition to the strong continental cooling over North East America and the general decrease in Tgrad spanning from mid to northern part of North America, might influence this strong Plumb flux anomaly in the North Pacific. Of note, sea-ice extent increases around East Siberia extending into the Chukchi Sea (not shown), highlighting the potential influence of sea ice variability on Tgrad and upward Plumb flux anomalies in the area.

Plotting the average Tgrad for various regions against the average number of SSWs for winters 1-3 (Fig. S6), we do see that the strongest Tgrad reduction occurs over the North East US in the

930 second winter, agreeing with the upward Plumb flux over the same region and serving as further

931 evidence for its contribution to the upward EP flux in winter 2. This Tgrad reduction continues

932 into the third winter where we also detected a reduction in the upward Plumb flux over the same

933 area (Fig. 8f). Looking towards the Barents Sea, a clear spatial difference emerges compared to

934 the North East US, where a clear Tgrad increase occurs in winter 3 related to the SSWs. In general

935 less changes are detected between winters in the North West NA and the North Pacific, reflecting

936 the confined cooling over higher latitudes in winter 3 associated with the SSWs.

937
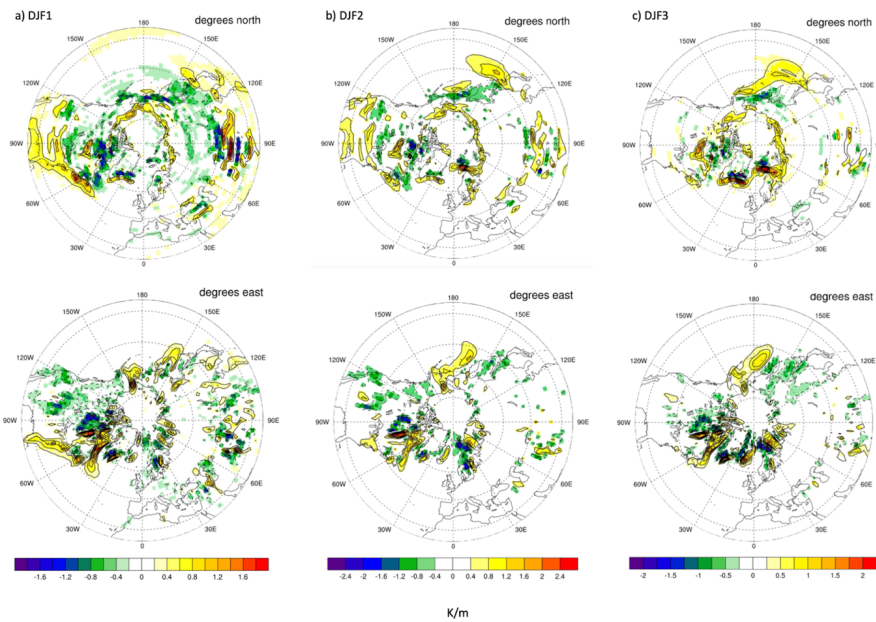
938

939 Figure 10: a-c) The zonal (degrees north) and meridional (degrees east) T2m gradient anomalies

940 (perturbed minus unperturbed) for winters 1-3. Contours indicate 95% significance according to a

941 Student's t-test. Note the different colorbar for each winter.

942

943 To complete our assessment of the tropospheric response, we examine if eddies play a role in the

944 *cpl* polar vortex response and the anomalous upward EP flux (Fig. 4a-f) as well as SSWs detected

945 in winter 3 by following Smith et al. (2022) (see Methods). This is done for both perturbed (red)

946 and unperturbed (blue) experiments in *cpl* and *atm-only* (Fig. S4). We see an increase in perturbed
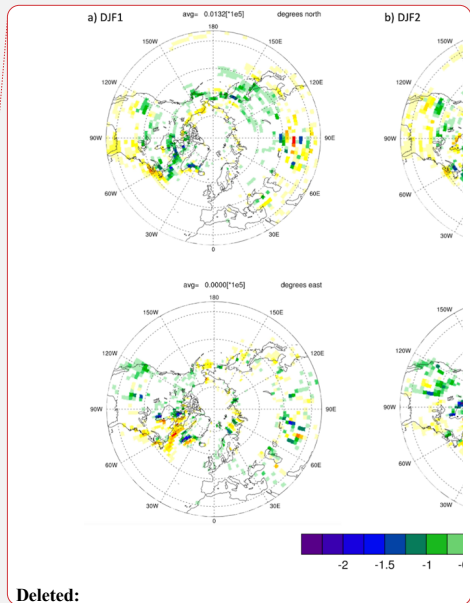
26

954 eddy feedback at around 40-70° N both for *cpl* winter 1 and winters 1-2 in *atm-only* during the
955 polar vortex strengthening (Fig. S4). However, the role of eddies in the polar vortex weakening in
956 winters 2-3 is unclear, especially considering the eddy feedback increase of the control run in
957 winter 2 (Fig. S4b). In general, these results suggest that the signal-to-noise ratio is too small to
958 identify a role for eddy feedback in our experiments.

959

960 **4 Discussion**

961 Our two sets of coupled ocean-atmosphere (*cpl*) and atmosphere-only (*atm-only*) experiments
962 examine the large-scale climate response to an idealized long-lasting NH eruption, where their
963 differences give us valuable insight into the volcanically forced mechanisms at play within the
964 coupled climate system in CESM1. Specifically, we analyzed the first three winters of the *cpl*
965 experiment and used the first two winters of *atm-only* as a comparison to investigate the dynamics
966 that govern the post-eruption stratospheric polar vortex and the associated surface response.
967 Results from the *cpl* experiment show a similar response in the first winter as in the two winters
968 of *atm-only*, with a strengthening of the zonal winds resulting from an aerosol-induced sharp
969 temperature gradient between the mid-latitudes and the pole (Fig. 4a and Fig. 5a). We show that
970 this zonal wind strengthening is not affected by the detected strong upward EP flux, where the LW
971 flux (Fig. 2e-f) supports our conclusions that the polar vortex strengthening is induced by the
972 thermal wind balance. A distinct change to this pattern emerges in *cpl* winter 2 where we detect an
973 SSW-like pattern, with strong negative anomalies emerging in the polar U50 winds and a warming
974 in the T50 field (Fig. 4b). We also detect an LW absorption at high latitudes, that is absent at
975 midlatitudes, where this T50 warming is evident of the potential role of a decreased temperature
976 gradient in the identified polar vortex weakening. Furthermore, the upward wave-activity flux
977 from the troposphere into the stratosphere and the T50 warming indicate absorption of upward
978 propagating waves into the stratosphere that causes this warming and weakening of U10 winds
979 over the polar cap. This pattern is known to be related to SSWs (Kretschmer et al., 2018; Kodera
980 et al., 2016) that we further confirm to occurr in winter 3. The strong upward EP flux greatly
981 depends on ocean-atmosphere coupling originating in the surface cooling in addition to the
982 changes in upper tropospheric zonal flow. This further contributes to the upward EP flux from the
983 troposphere into the stratosphere that eventually leads to polar vortex weakening and enhanced
984 SSWs.

27

Deleted: Discussions

Formatted: English (US)

Deleted: We assessed

Formatted: Font: Italic

Deleted: our

Deleted: detected

Formatted: English (US)

Deleted: e

Deleted: in the LW flux

Deleted: identified

Deleted: in winter 3.

993 Although the above coincides with a positive (negative) eddy feedback in the first (second) winter

994 that could in theory play a role in sustaining the strengthening (weakening) of the polar vortex, our

995 eddy feedback results indicate low signal-to-noise ratio where further studies with additional

996 ensemble members would be required to confirm their role in the forced response. We also note

997 that Smith et al. (2022) identified CESM1 WACCM-SC as having one of the weakest eddy

998 feedback of the sixteen models they investigated, so the response of eddy feedback may be more

999 significant in other models. Similar to the eddy feedback, low signal-to-noise ratio is also evident

1000 in the SSW analysis. However, the response we detect in the U50 and T50 fields is strong compared

1001 to the unperturbed simulation where the SSWs provide an explanation in agreement with the

1002 patterns detected. Furthermore, the SSW analysis for *atm-only* and the ensemble size test (Fig. 7)

1003 both show strong evidence of a robust signal for winter 3 despite the noisy polar vortex and the

1004 limited ensemble size. We also see that the large decrease in SSWs in the perturbed simulation of

1005 *atm-only* (when compared to unperturbed) is consistent with the detected polar vortex

1006 strengthening. This further supports the significance of the signal we detect in *cpl* winter 3

1007 compared to the background noise. In addition, all winters examined, in both *cpl* and *atm-only*,

1008 showed that there is up to 15% chance of getting more than 1 SSWs per winter in all ensemble

1009 members. This is not far from Ineson et al. (2022) who identified a double event once every 9 years

1010 in a 66-year ERA5 record. The exception is *cpl* winter 3 that is also the only winter that has 3

1011 SSWs, with the average SSW occurrence also being the only winter above 1 (1.17) while all other

1012 winters span between 0.15-0.85 per winter. A similar NH high-latitude eruption has not taken place

1013 during the observational period, so we have no comparison. Also, to the best of our knowledge, a

1014 similar high-latitude sulfur injection study has not been performed before. Therefore, it is difficult

1015 to say at this stage if such a response is realistic or not, but in general more than two SSWs per

1016 winter can be considered exceptional yet plausible, as is also the case for our idealized eruption.

1017

1018 Bittner et al. (2016b) identified an opposite response driven by a similar underlying mechanism,

1019 when compared to our *cpl* response in winters 2-3 (Fig. 4), following a Tambora-like eruption

1020 where a strengthening of the polar vortex due to less wave breaking at high latitudes was

1021 considered to be an indirect effect associated with a changes in planetary wave propagation. Since

1022 the volcanic aerosols in our experiments have declined extensively in the third winter, making the

1023 aerosol thermal forcing a limited factor, we cannot rule out similar indirect effects where changes

28

in wave propagation leads to an increase in wave breaking at high latitudes and hence the increase in SSWs.

While not directly comparable to our study but still providing an important analog, Muthers et al. (2016) identified an average increase in the number of SSWs during a 30-year (constant) decrease in solar radiation in line with our significant increase in SSWs in winter 3. Our results do support the findings of Sjolte et al. (2019), where the stratospheric temperature gradient does not appear to play a major role in the polar vortex weakening we identify, while the upward wave flux does. The strong surface cooling detected in Fig. 8 is a well-known caveat in CMIP5 models (including CESM1) (Driscoll et al., 2012; Chylek et al., 2020) and is clearly detected in our coupled simulations. Since our results indicate the dominant role of the volcanically induced stratospheric thermal wind response that causes the polar vortex strengthening, the cooling does not appear to impact the response identified in winter 1. This is also revealed by the EP flux. The same cannot be said about winters 2-3, where our results indicate that the exaggerated spatiotemporal T2m pattern might explain the strong upward wave flux and the associated stratospheric response. Interestingly, a slight difference between *atm-only* and *cpl* is detected in both the LW and SW flux that is caused by a strong significant decrease in high cloud cover in the *cpl* simulation (not shown). This cloud cover decrease, especially at mid- to high latitudes, agrees with the increased LW fluxes at higher latitudes in addition to the decrease in SW flux and the associated surface cooling. This raises a question regarding the role of forced surface processes in these high cloud changes, which we leave open for further studies.

As mentioned in the methods section, we assume a similar lifetime of volcanic aerosols at 65° N as at 45° N. When considering the e-folding time in Toohey et al. (2019), a substantial aerosol decrease of about 43% occurs at 17km (a.b.s.) for an eruption at 60° compared to at 0°. However, since our experiment assumes a constant stratospheric injection over 5 months with the aim to simulate a long-lasting HL eruption compared to a single injection at low latitudes, the difference in the e-folding time between low and high-latitudes would be expected to decrease. Using CESM2-WACCM6 with interactive chemistry Zhuo et al. (2023) identified that although an eruption at 64° N did have a shorter aerosol lifetime compared to one at 15° N, it leads to stronger volcanic forcing over the NH extratropics. In addition, one of their conclusions was that different duration and intensity of both tropical and NH extratropical eruptions can lead to different results,

Deleted: but rather

Deleted: 7

Deleted: the

Deleted: simulation

Deleted: balance

Deleted: as

Deleted: in addition to the eddy feedback although weakly

Formatted: English (US)

Deleted:

Deleted: .,

Deleted: they lead

Deleted: although the resulting climate impacts did not last as long

29

stressing that our 6 month long stratospheric sulfate aerosol enhancement is not directly comparable with volcanic eruptions of shorter duration. Although the aerosol lifetime in our experiment might be exaggerated into the third year, our results do indicate that the polar vortex weakening in winter 2 appears to act as a trigger for further weakening that eventually leads to SSWs in winter 3. In order to increase confidenceprecu on such a delayed link, additional sensitivity simulations are required, which we we leave that for future studies.

Unlike our eruption simulated using a version of WACCM4, where the chemistry is prescribed, natural volcanic eruptions can contain various chemical compounds that impact the formation and the lifetime of sulfate aerosols as well as affect the atmospheric circulation via, e.g., ozone depletion, like halogens are known to do. More advanced versions as well as models that include interactive chemistry are thus important to reveal in more detail the chemistry-climate interactions that occur in the natural world (Clyne et al., 2021; Case et al., 2023; Fuglestvedt et al., 2024). Thus our idealized experiment can be considered primitive in the sense that it only considers sulfate aerosols but sufficient when focusing on answering questions on the basic mechanism that such eruptions can initiate. Another important aspect that we do not focus on in our study is the role of different initial conditions on the forced climate response, where initial atmospheric and climate conditions, including e.g. the stability of the polar vortex, control the lifetime and distribution of the volcanic aerosols as well as the forced dynamic climate response (Zanchettin et al., 2019; Weierbach et al., 2023; Zhuo et al., 2023; Fuglestvedt et al., 2024). An exception is our assessment on how the easterly and westerly phase of the QBO affect our results where we compared ensemble members showing easterly phase with the westerly ones to test if the U50 and T50 response patterns would be different. They were not; both phases showed a weakening of the U50 although the zonal winds were more confined and consistent over the higher latitudes of the NH during the easterly phase (not shown). The difference in the number of ensemble members used for these calculations could of course impact the statistics of this test of ours but not the overall pattern detected.

CESM2-WACCM6 has obvious improvements when compared to CESM1-WACCM4 (see e.g. Gettleman et al., 2019, Danabasoglu et al., 2020), among them being an interactive QBO as well as having a slightly higher frequency of SSW occurrence (Holland et al., 2024). Nonetheless, CESM1-WACCM4 has comparable transient climate response to CESM2 as well as the ability to

capture the general physical mechanism occurring within the climate system as identified in various recent studies (Danabasoglu et al., 2020; Zang et al., 2018; Elsbury et al., 2021b; Peings et al., 2023; Ding et al., 2023; Yu et al., 2024).

5 Conclusions

Through comparison of the *cpl* and *atm-only* simulations, our results clearly demonstrates the important role of ocean-atmosphere coupling in the stratospheric response to enhancements of the stratospheric sulfate aerosol layer at higher NH latitudes. We see that this aerosol enhancement layer triggers two competing mechanisms in the first three winters:

i) Winter 1: The stratospheric polar vortex strengthening is triggered by stratospheric aerosol thermal forcing via thermal wind balance. This response is not influenced by the strong upward wave flux identified, originating in the forced surface cooling and changes in tropospheric circulation, and provides strong evidence of two mechanisms that are competing simultaneously: A Top-down and a Bottom-up mechanism, where the Top-down mechanism dominates the response.

ii) Winter 2: The upward wave flux is absorbed in the stratosphere that causes a warming over the polar cap and a polar vortex weakening. This pattern is similar to SSWs although its occurrence is not significant. Here the Bottom-up mechanism dominates.

iii) Winter 3: The persistence of the upward wave flux continuing into the third winter leads to an increase in SSWs with warming now confined over the polar cap, again demonstrating the dominating Bottom-up mechanism as in winter 2.

It is clear from our results that the strong surface cooling following the HL sulphate aerosol injection causes dramatic changes in tropospheric circulation. These changes further modify atmospheric waveguides where we detect an increase in propagation of planetary waves in the lower stratosphere occurring at higher latitudes. Although we do find similarities in the eddy feedback when compared to the general climate signal that we identify, such as the decrease in eddy feedback in winter 1 potentially sustaining the polar vortex strengthening, we emphasize its weak signal. At the same time we encourage further studies on this subject, especially concerning the lack of published comparison studies regarding both high and low latitude volcanic eruptions and SSWs. Ideally such studies would include the latest model generations in addition to observational datasets. They should also consider the impact of different climate realizations and

1162 the eruption magnitude on the forced response. Furthermore, these results highlight the importance

1163 of including high-latitude volcanic forcing simulations of various lengths and/or magnitudes in

1164 projects such as VolMIP, especially considering the current volcanic unrest and increased activity

1165 in some of the major volcanic systems in Iceland.

1166 Currently, work is ongoing to test the sensitivity of the polar vortex and the emerging SSWs to NH

1167 eruptions that are smaller in magnitude as well as the long-term climate impacts.

1168

1169 **Data availability**

1170 The model output is available upon request by contacting the corresponding author.

1171

1172 **Author contribution**

1173 HG conceptualized this study along with GM, YP and DZ. *cpl* and *atm-only* experiments were

1174 carried out by HG and YP. Analysis and calculations of model output as well as graphical

1175 representation was done by HG except for the eddy feedback and the probability of favorable

1176 propagation conditions that was done by YP and the ensemble size test that was done by DZ.

1177 Manuscript draft was done by HG and editing was done by DZ and YP. GM served as the principal

1178 investigator of this work and did the final editing.

1179

1180

1181 **Competing interests**

1182 The corresponding author declares that none of the authors have any competing interest.

1183

1184 **Acknowledgement**

assistance during this work HG's stay at UCI. Finally, we also want to thank Matthew Toohey for his assistance in the interpolation of the forcing files for WACCM4.

References

Azoulay, A., Schmidt, H., & Timmreck, C. The Arctic polar vortex response to volcanic forcing of different strengths. *J Geophys Res-Atmos*, *126*(11), e2020JD034450. (2021).

Baldwin, M. P., & Dunkerton, T. J. Propagation of the Arctic Oscillation from the stratosphere to the troposphere. *J Geophys Res-Atmos*, *104*(D24), 30937-30946. (1999).

Barsotti, S., Di Rienzo, D. I., Thordarson, T., Björnsson, B. B., & Karlsdóttir, S. Assessing impact to infrastructures due to tephra fallout from Öræfajökull volcano (Iceland) by using a scenario-based approach and a numerical model. *Front Earth Sci*, *6*, 196. (2018).

Bittner M, Schmidt H, Timmreck C, Sienz F. Using a large ensemble of simulations to assess the Northern Hemisphere stratospheric dynamical response to tropical volcanic eruptions and its uncertainty. *Geophys Res Lett*, 43(17), 9324–32. (2016).

Brayshaw, D. J., B. Hoskins, and M. Blackburn. The basic ingredients of the North Atlantic storm track. Part I: Land–sea contrast and orography. *J. Atmos. Sci.*, **66**, 2539–2558, https://doi.org/10.1175/2009JAS3078.1. (2009).

Brown, F., Marshall, L., Haynes, P. H., Garcia, R. R., Birner, T., & Schmidt, A. On the magnitude and sensitivity of the quasi-biennial oscillation response to a tropical volcanic eruption. *Atmos. Chem. Phys*, *23*(9), 5335-5353. (2023).

Brugnatelli, V., & Tibaldi, A. Effects in North Africa of the 934–940 CE Eldgjá and 1783–1784 CE Laki eruptions (Iceland) revealed by previously unrecognized written sources. *B. Volcanol*, *82*(11), 73. (2020).

33

Case, P., Colarco, P. R., Toon, B., Aquila, V., & Keller, C. A. Interactive stratospheric aerosol microphysics-chemistry simulations of the 1991 Pinatubo volcanic aerosols with newly coupled sectional aerosol and stratosphere-troposphere chemistry modules in the NASA GEOS Chemistry-Climate Model (CCM). *J Adv. Model Earth Sy.*, *15*(8), e2022MS003147. (2023).

Charlton-Perez AJ, Ferranti L, Lee RW. The influence of the stratospheric state on North Atlantic weather regimes. Quart. J. Roy. Meteor. Soc, 144:1140–1151. https://doi.org/10.1002/qj.3280 (2018).

Charlton, A. J., & Polvani, L. M. A new look at stratospheric sudden warmings. Part I: Climatology and modeling benchmarks. *J. Climate*, *20*(3), 449-469. (2007).

Church, J.A., White, N.J., Arblaster, J.M. Significant decadal-scale impact of volcanic eruptions on sea level and ocean heat content. *Nature* 438 (7064), 74–77. (2005).

Chylek, P., Folland, C., Klett, J. D., & Dubey, M. K. CMIP5 climate models overestimate cooling by volcanic aerosols. *Geophys. Res. Lett*, *47*(3), e2020GL087047. (2020).

Clyne, M., Lamarque, J.-F., Mills, M. J., Khodri, M., Ball, W., Bekki, S., Dhomse, S. S., Lebas, N., Mann, G., Marshall, L., Niemeier, U., Poulain, V., Robock, A., Rozanov, E., Schmidt, A., Stenke, A., Sukhodolov, T., Timmreck, C., Toohey, M., Tummon, F., Zanchettin, D., Zhu, Y., and Toon, O. B.: Model physics and chemistry causing intermodel disagreement within the VolMIP-Tambora Interactive Stratospheric Aerosol ensemble, Atmos. Chem. Phys., 21, 3317–3343, https://doi.org/10.5194/acp-21-3317-2021, (2021).

Colose CM, LeGrande AN, Vuille M. Hemispherically asymmetric volcanic forcing of tropical hydroclimate during the last millennium. *Earth Sys Dyn*. 7(3), 681–96. doi:10.5194/esd-7-681-2016 (2016).

DallaSanta, K., Gerber, E. P., & Toohey, M. The circulation response to volcanic eruptions: The key roles of stratospheric warming and eddy interactions. *J. Clim*, *32*(4), 1101-1120. (2019).

34

1311

DallaSanta, K., & Polvani, L. M. Volcanic stratospheric injections up to 160 Tg (S) yield a Eurasian winter warming indistinguishable from internal variability. *Atm. Chem. Phys*, *22*(13), 8843-8862 (2022).

Danabasoglu, G., Lamarque, J. F., Bacmeister, J., Bailey, D. A., DuVivier, A. K., Edwards, J., ... & Strand, W. G. The community earth system model version 2 (CESM2). *J Adv. Model Earth Sy*, *12*(2), e2019MS001916 (2020).

Dee, S. G., Cobb, K. M., Emile-Geay, J., Ault, T. R., Edwards, R. L., Cheng, H., & Charles, C. D. No consistent ENSO response to volcanic forcing over the last millennium. *Science*, *367*(6485), 1477-1481 (2020).

Ding, X., Chen, G., Zhang, P., Domeisen, D. I., & Orbe, C. Extreme stratospheric wave activity as harbingers of cold events over North America. *Commun. Earth Environ*, *4*(1), 187 (2023).

Domeisen, D. I., Grams, C. M., & Papritz, L. The role of North Atlantic–European weather regimes in the surface impact of sudden stratospheric warming events. *Weather Clim. Dynam*, *1*(2), 373-388 (2020).

Driscoll, S., Bozzo, A., Gray, L. J., Robock, A., Stenchikov, G. Coupled ModelIntercomparison Project 5 (CMIP5) simulations of climate following volcanic erup-tions. *J. Geophys. Res. Atmos*, 117 (D17) (2012).

Edmon, H.J., Hoskins, B.J. and McIntyre, M.E. Eliassen-Palm cross sections for the troposphere. *J. Atmos. Sci*, **37**, 2600–2616 (1980).

Einarsson, P. Historical accounts of pre-eruption seismicity of Katla, Hekla, Öræfajökull and other volcanoes in Iceland. *Jökull*, *69*, 35-52 (2019).

1340

Elsbury, D., Y. Peings and G. Magnusdottir. Variation in the Holton-Tan effect by longitude. Q. J. Roy. Meteor. Soc. DOI: 10.1002/qj.3993 (2021b).

Elsbury, D., Peings, Y., & Magnusdottir, G. CMIP6 models underestimate the Holton-Tan effect. *Geophys. Res. Lett*, *48*(24), e2021GL094083 (2021).

Fischer, H., Siggaard-Andersen, M.L., Ruth, U., Röthlisberger, R., Wolff, E. Glacial/interglacial changes in mineral dust and sea-salt records in polar ice cores: Sources,transport, and deposition. *Rev. Geophys*. (1), 45 (2007).

Fuglestvedt, H. F., Zhuo, Z., Toohey, M., & Krüger, K. Volcanic forcing of high-latitude Northern Hemisphere eruptions. *npj Clim. Atmos. Sci*, *7*(1), 10 (2024).

Gettelman, A., Mills, M. J., Kinnison, D. E., Garcia, R. R., Smith, A. K., Marsh, D. R., ... & Randel, W. J. The whole atmosphere community climate model version 6 (WACCM6). *J. Geophys. Res-Atmos*, *124*(23), 12380-12403 (2019).

Gettelman, A., Schmidt, A., & Egill Kristjánsson, J. Icelandic volcanic emissions and climate. *Nature Geosci*, *8*(4), 243-243 (2015).

Gleckler, P.J., AchutaRao, K., Gregory, J.M., Santer, B.D., Taylor, K.E., Wigley, T.M.L. Krakatoa lives: The effect of volcanic eruptions on ocean heat content and thermal expansion. Geophys. Res. Lett. (17), 33 (2006).

Graf, H.F., Perlwitz, J., Kirchner, I. Northern hemisphere tropospheric midlatitude circulation after violent volcanic eruptions. Contr. Atmos. Physics 67 (1), 3–13 (1994).

Graf, H.-F., D. Zanchettin, C. Timmreck and M. Bittner. Observational constraints on the tropospheric and near-surface winter signature of the Northern Hemisphere stratospheric polar vortex. Clim. Dyn., 43, 3245, doi:10.1007/s00382-014-2101-0 (2014).

Guðlaugsdóttir, H., Steen-Larsen, H. C., Sjolte, J., Masson-Delmotte, V., Werner, M., & Sveinbjörnsdóttir, Á. E. The influence of volcanic eruptions on weather regimes over the North Atlantic simulated by ECHAM5/MPI-OM ensemble runs from 800 to 2000 CE. *Atm. Res*, *213*, 211-223 (2018).

Guðlaugsdóttir, H., Sjolte, J., Sveinbjörnsdóttir, Á. E., Werner, M., & Steen-Larsen, H. C. North Atlantic weather regimes in δ18O of winter precipitation: isotopic fingerprint of the response in the atmospheric circulation after volcanic eruptions. *Tellus B*, *71*(1), 1633848 (2019).

Haynes, P. H. Stratospheric dynamics. *Ann. Rev. Fluid Mech.* *37(1), 263-293, doi: 10.1146/annurev.fluid.37.061903.175710* (2005).

He, Y., Huang, J. & Ji, M. Impact of land–sea thermal contrast on interdecadal variation in circulation and blocking. *Clim Dyn* **43**, 3267–3279, https://doi.org/10.1007/s00382-014-2103-y *(2014).*

Holland, M. M., Hannay, C., Fasullo, J., Jahn, A., Kay, J. E., Mills, M., ... & Bailey, D. New model ensemble reveals how forcing uncertainty and model structure alter climate simulated across CMIP generations of the Community Earth System Model. *Geosci. Model Dev*, *17*(4), 1585-1602 (2024).

Hoskins, B. J., and P. J. Valdes. On the existence of storm-tracks. *J. Atmos. Sci.*, **47**, 1854–1864, https://doi.org/10.1175/1520-0469(1990)047<1854:OTEOST>2.0.CO;2 (1990).

Huang, J., Hitchcock, P., Maycock, A. C., McKenna, C. M., & Tian, W. Northern hemisphere cold air outbreaks are more likely to be severe during weak polar vortex conditions. *Commun. Earth Environ*, *2*(1), 147 (2021).

Hurrell, J.W. Decadal trends in the north atlantic oscillation: regional tempera-tures and precipitation. Science 269 (5224), 676–679 (1995).

Hurrell, J. W., Holland, M. M., Gent, P. R., Ghan, S., Kay, J. E., Kushner, P. J., ... & Marshall, S. The community earth system model: a framework for collaborative research. *B. Am. Meteorol. Soc*, *94*(9), 1339-1360. (2013).

Ineson, S., Dunstone, N. J., Scaife, A. A., Andrews, M. B., Lockwood, J. F., & Pang, B. Statistics of sudden stratospheric warmings using a large model ensemble. *Atmos. Sci. Lett*, *25*(3), e1202. (2024).

Jungclaus, J. H., Bard, E., Baroni, M., Braconnot, P., Cao, J., Chini, L. P., Egorova, T., Evans, M., González-Rouco, J. F., Goosse, H., Hurtt, G. C., Joos, F., Kaplan, J. O., Khodri, M., Klein Goldewijk, K., Krivova, N., LeGrande, A. N., Lorenz, S. J., Luterbacher, J., Man, W., Maycock, A. C., Meinshausen, M., Moberg, A., Muscheler, R., Nehrbass-Ahles, C., Otto-Bliesner, B. I., Phipps, S. J., Pongratz, J., Rozanov, E., Schmidt, G. A., Schmidt, H., Schmutz, W., Schurer, A., Shapiro, A. I., Sigl, M., Smerdon, J. E., Solanki, S. K., Timmreck, C., Toohey, M., Usoskin, I. G., Wagner, S., Wu, C.-J., Yeo, K. L., Zanchettin, D., Zhang, Q., and Zorita, E.: The PMIP4 contribution to CMIP6 – Part 3: The last millennium, scientific objective, and experimental design for the PMIP4 past1000 simulations, Geosci. Model Dev., 10, 4005-4033, https://doi.org/10.5194/gmd-10-4005-2017, (2017).

Karami, K., Braesicke, P., Sinnhuber, M., and Versick, S. On the climatological probability of the vertical propagation of stationary planetary waves, Atmos. Chem. Phys., 16, 8447–8460, https://doi.org/10.5194/acp-16-8447-2016 (2016).

Khodri, M., Izumo, T., Vialard, J., Janicot, S., Cassou, C., Lengaigne, M., et al. Tropical explosive volcanic eruptions can trigger El Niño by cooling tropical Africa. *Nat. Commun*, 8(1), 778. https://doi.org/10.1038/s41467-017-00755-6 (2017).

Kim, B.M., Son, S.W., Min, S.K., Jeong, J.H., Kim, S.J., Zhang, X., Shim, T., Yoon, J.H. Weakening of the stratospheric polar vortex by arctic sea-ice loss. Nat.Commun. 5, 4646 (2014).

Kodera, K. Influence of volcanic eruptions on the troposphere through strato-spheric dynamical processes in the northern hemisphere winter. J. Geophys. Res.-Atmos. 99 (D1), 1273–1282 (1994).

Kodera, K., Mukougawa, H., Maury, P., Ueda, M., & Claud, C. Absorbing and reflecting sudden stratospheric warming events and their relationship with tropospheric circulation. *J. Geophys. Res-Atmos*, *121*(1), 80-94 (2016).

Kolstad, E. W., Lee, S. H., Butler, A. H., Domeisen, D. I., & Wulff, C. O. Diverse surface signatures of stratospheric polar vortex anomalies. *J. Geophys. Res-Atmos*, *127*(20), e2022JD037422 (2022).

Kretschmer, M., Cohen, J., Matthias, V., Runge, J., & Coumou, D. The different stratospheric influence on cold-extremes in Eurasia and North America. *npj Clim. Atmos. Sci*, *1*(1), 44 (2018).

Labe, Z., Peings, Y., & Magnusdottir, G. The effect of QBO phase on the atmospheric response to projected Arctic sea ice loss in early winter. *Geophys. Res. Lett.*, *46*(13), 7663-7671 (2019).

Larsen, G., & Gudmundsson, M. T. Volcanic system: Bárðarbunga system. *Catalogue of Icelandic Volcanoes*, 1-11 (2014).

Lehtonen, I., & Karpechko, A. Y. Observed and modeled tropospheric cold anomalies associated with sudden stratospheric warmings. *J. Geophys. Res-Atmos.*, *121*(4), 1591-1610 (2016).

Ma, J., Chen, W., Yang, R. et al. Downward propagation of the weak stratospheric polar vortex events: the role of the surface arctic oscillation and the quasi-biennial oscillation. Clim. Dyn. 62, 4117–4131 https://doi.org/10.1007/s00382-024-07121-5 (2024).

Matsuno, T. Vertical propagation of stationary planetary waves in the winter Northern Hemisphere, J. Atmos. Sci., 27, 871–883. 32291, 32292, 32294, 32296, 32306 (1970).

Meronen, H., Henriksson, S. V., Räisänen, P., & Laaksonen, A. Climate effects of northern hemisphere volcanic eruptions in an Earth System Model. *Atmos. Res.*, *114*, 107-118 (2012).

Muthers, S., Raible, C. C., Rozanov, E., & Stocker, T. F. Response of the AMOC to reduced solar radiation–the modulating role of atmospheric chemistry. *Earth Syst. Dynam.*, 7(4), 877-892 (2016).

Nakamura, N. Large-Scale Eddy-Mean Flow Interaction in the Earth's Extratropical Atmosphere. *Annu. Rev. Fluid Mech.*, 56(1), 349-377 (2024).

Neely III, R. R., Conley, A. J., Vitt, F., & Lamarque, J. F. A consistent prescription of stratospheric aerosol for both radiation and chemistry in the Community Earth System Model (CESM1). *Geosci. Model Dev.*, 9(7), 2459-2470 (2016).

Oman, L., Robock, A., Stenchikov, G., Schmidt, G. A., & Ruedy, R. Climatic response to high-latitude volcanic eruptions. *J. Geophys. Res-Atmos*, 110(D13) (2005).

Omrani, N.-E., Keenlyside, N., Matthes, K., Boljka, L., Zanchettin, D., Jungclaus, J. H., Lubis, S. W. Coupled stratosphere-troposphere-Atlantic multidecadal oscillation and its importance for near-future climate projection. *npj Clim. Atmos. Sci*, 5, 59, https://doi.org/10.1038/s41612-022-00275-1 (2022).

Oppenheimer, C., Orchard, A., Stoffel, M., Newfield, T. P., Guillet, S., Corona, C., ... & Büntgen, U. The Eldgjá eruption: timing, long-range impacts and influence on the Christianisation of Iceland. *Climatic Change*, 147, 369-381.Otterå, O.H., Bentsen, M., Drange, H., Suo, L., 2010. External forcing as a metronome foratlantic multidecadal variability. Nat. Geosci. 3 (10), 688–694 (2018).

Ortega, P., Swingedouw, D., Masson-Delmotte, V., Risi, C., Vinther, B., Yiou, P., Vautard,R., Yoshimura, K. Characterizing atmospheric circulation signals in. Greenlandice cores: insights from a weather regime approach. Clim. Dyn. 43 (9–10), 2585–2605 (2014).

Otterå, O. H., Bentsen, M., Drange, H., & Suo, L. External forcing as a metronome for Atlantic multidecadal variability. *Nat. Geosci*, *3*(10), 688-694 (2010).

Pausata, F. S. R., Chafik, L., Caballero, R. & Battisti, D. S. Impacts of high- latitude volcanic eruptions on ENSO and AMOC. Proc. Natl Acad. Sci. 112, 13784–13788 (2015).

Pausata, F.S.R., Zanchettin, D., Karamperidou, C., Caballero, R., Battisti, D. S. ITCZ shift and extratropical teleconnections drive ENSO response to volcanic eruptions. Sci. Adv. 6(23) eaaz5006, doi: 10.1126/sciadv.aaz5006 (2020).

Pausata, F. S. R., Zhao, Y., Zanchettin, D., Caballero, R., & Battisti, D. S. Revisiting the mechanisms of ENSO response to tropical volcanic eruptions. Geophys. Res. Lett., 50, e2022GL102183. https://doi.org/10.1029/2022GL102183 (2023).

Perlwitz, J., Graf, H.F. The statistical connection between tropospheric and. stra-tospheric circulation of the Northern Hemisphere in winter. J. Clim. (10),2281–2295 (1995).

Peings, Y., & Magnusdottir, G. Response of the wintertime Northern Hemisphere atmospheric circulation to current and projected Arctic sea ice decline: A numerical study with CAM5. *J. Clim.*, *27*(1), 244-264 (2014).

Peings, Y., Davini, P., & Magnusdottir, G. Impact of Ural blocking on early winter climate variability under different Barents-Kara sea ice conditions. *J. Geophys. Res-Atmos*, *128*(6), e2022JD036994 (2023).

Plumb, R. A. On the three-dimensional propagation of stationary waves. *J. Atmos. Sci.*, *42*(3), 217-229 (1985).

Polvani, L. M., Banerjee, A., & Schmidt, A. Northern Hemisphere continental winter warming following the 1991 Mt. Pinatubo eruption: reconciling models and observations. *Atmos. Chem. Phys*, *19*(9), 6351-6366 (2019).

41

Portal, A., Pasquero, C., D'andrea, F., Davini, P., Hamouda, M. E., & Rivière, G. Influence of reduced winter land–sea contrast on the midlatitude atmospheric circulation. *J. Clim.*, *35*(19), 6237-6251. (2022).

Predybaylo, E., Stenchikov, G., Wittenberg, A. T. & Osipov, S. El Niño/ Southern Oscillation response to low-latitude volcanic eruptions depends on ocean pre-conditions and eruption timing. Commun. Earth Environ. 1, 1–13 (2020).

Rayner, N. A. A., Parker, D. E., Horton, E. B., Folland, C. K., Alexander, L. V., Rowell, D. P., ... & Kaplan, A. Global analyses of sea surface temperature, sea ice, and night marine air temperature since the late nineteenth century. *J. Geophys. Res-Atmos*, *108*(D14) (2003).

Robock, A., Mao, J. Winter warming from large volcanic eruptions. Geophys. Res.Lett. 19 (24), 2405–2408. (1992).

Robock, A. Volcanic eruptions and climate. Rev. Geophys. 38 (2), 191–219. (2000).

Screen, J. A., Deser, C., Smith, D. M., Zhang, X., Blackport, R., Kushner, P. J., ... & Sun, L. Consistency and discrepancy in the atmospheric response to Arctic sea-ice loss across climate models. *Nat. Geosci.*, *11*(3), 155-163. (2018).

Shindell, D.T., Schmidt, G.A., Mann, M.E., Faluvegi, G. Dynamic winter. Climate response to large tropical volcanic eruptions since 1600. J. Geophys. Res.-Atmos.(D5), 109.Sigl, M., Winstrup, M., McConnell, J.R., Welten, K.C., Plunkett, G., Ludlow, F., Buntgen,U., Caffee, M., Chellman, N., Dahl-Jensen, D., Fischer, H., 2009. Timing and climate forcing of volcanic eruptions for the past 2500 years. Nature 523 (7562), 543–549 (2009).

Sjolte, J., Adolphi, F., Guðlaugsdòttir, H., & Muscheler, R. Major Differences in Regional Climate Impact Between High-and Low-Latitude Volcanic Eruptions. *Geophys. Res. Lett.*, *48*(8), e2020GL092017. (2021).

Smith, D. M., Eade, R., Andrews, M. B., Ayres, H., Clark, A., Chripko, S., ... & Walsh, A. Robust but weak winter atmospheric circulation response to future Arctic sea ice loss. *Nat. Commun.*, *13*(1), 727, (2022)..

Smith, K. L., Neely, R. R., Marsh, D. R., & Polvani, L. M. The specified chemistry whole atmosphere community climate model (SC-WACCM). *J. Adv. Model. Earth Sy.*, *6*(3), 883-901, (2014).

Stenchikov, G., Robock, A., Ramaswamy, V., Schwarzkopf, M.D., Hamilton, K.,Ramachandran, S., Arctic Oscillation response to the 1991 Mount Pinatubo.eruption: Effects of volcanic aerosols and ozone depletion. J. Geophys. Res.-Atmos.(D24), 107, (2002).

Stenchikov, G., Delworth, T.L., Ramaswamy, V., Stouffer, R.J., Wittenberg, A., Zeng, F., Volcanic signals in oceans. J. Geophys. Res.-Atmos. (D16), 114, (2009).

Stothers, R. B. Far reach of the tenth century Eldgjá eruption, Iceland. *Climatic Change*, *39*(4), 715-726, (1998).

Swingedouw, D., Ortega, P., Mignot, J., Guilyardi, E., Masson-Delmotte, V., Butler, P.G.,Khodri, M., Séférian, R., Bidecadal North Atlantic ocean circulation variability controlled by timing of volcanic eruptions. Nat. Commun. 6, 6545, (2015).

Thomas, M. A., Giorgetta, M. A., Timmreck, C., Graf, H. F., & Stenchikov, G., Simulation of the climate impact of Mt. Pinatubo eruption using ECHAM5–Part 2: Sensitivity to the phase of the QBO and ENSO. *Atmos. Chem. Phys*, *9*(9), 3001-3009, (2009).

Timmreck, C.: Modeling the climatic effects of large explosive volcanic eruptions, Wiley Interdisciplinary Reviews: Climate Change, 3, 545–564, (2012).

Deleted: (2022).
Deleted: *Nature communications*,
Deleted: .
Deleted: (2014).
Deleted: *Journal of Advances in Modeling*
Deleted: *Systems*
Deleted: .
Deleted: ., 2002
Deleted: .
Deleted: .,2009
Deleted: .
Deleted: (1998).
Deleted: .
Deleted: ., 2015
Deleted: .
Deleted: (2009).
Deleted: *Atmospheric Chemistry and Physics*
Deleted: .
Deleted: .

Thordarson, T., & Self, S. Atmospheric and environmental effects of the 1783–1784 Laki eruption: A review and reassessment. *J. Geophys. Res.-Atmos.*, *108*(D1), AAC-7 (2003).

Thordarson, T., Miller, D. J., Larsen, G., Self, S., & Sigurdsson, H. New estimates of sulfur degassing and atmospheric mass-loading by the 934 AD Eldgjá eruption, Iceland. *J. Volcanol. Geoth. Res.*, *108*(1-4), 33-54 (2001).

Toohey, M., Stevens, B., Schmidt, H., & Timmreck, C. Easy Volcanic Aerosol (EVA v1. 0): an idealized forcing generator for climate simulations. *Geosci. Model Dev.*, *9*(11), 4049-4070 (2016).

Toohey, M., Krüger, K., Schmidt, H., Timmreck, C., Sigl, M., Stoffel, M., & Wilson, R. Disproportionately strong climate forcing from extratropical explosive volcanic eruptions. *Nat. Geosci*, 12(2), 100-107 (2019).

Toohey, M., Krüger, K., Bittner, M., Timmreck, C., and Schmidt, H.: The impact of volcanic aerosol on the Northern Hemisphere stratospheric polar vortex: mechanisms and sensitivity to forcing structure, Atmos. Chem. Phys., 14, 13063–13079, https://doi.org/10.5194/acp-14-13063-2014, (2014).

Wake, B. Land–sea contrast. *Nat. Clim. Change* 4, 326, https://doi.org/10.1038/nclimate2233 (2014).

Weierbach, H., LeGrande, A. N., and Tsigaridis, K.: The impact of ENSO and NAO initial conditions and anomalies on the modeled response to Pinatubo-sized volcanic forcing, Atmos. Chem. Phys., 23, 15491–15505, https://doi.org/10.5194/acp-23-15491-2023, (2023).

Yu, Q., Wu, B., & Zhang, W. The atmospheric connection between the Arctic and Eurasia is underestimated in simulations with prescribed sea ice. *Commun.* Earth *Environ.*, *5*(1), 435 (2024).

Zambri, B., Robock, A., Mills, M. J., & Schmidt, A. Modeling the 1783–1784 Laki eruption in Iceland: 2. Climate impacts. *J. Geophys. Res.-Atmos*, *124*(13), 6770-6790 (2019).

Zambri B, Slawinska J, Robock A, LeGrande AN. Northern Hemisphere Winter Warming and Summer Monsoon Reduction after Volcanic Eruptions over the Last Millennium. J Geophys Res Atmos, 122 (15) :7971-7989. doi: 10.1002/2017jd026728 (2017).

Zanchettin, D., Timmreck, C., Graf, H.F., Rubino, A., Lorenz, S., Lohmann, K., Jungclaus,J.H, Bi-decadal variability excited in the coupled ocean-atmosphere system by strong tropical volcanic eruptions. Clim. Dyn. 39 (1–2), 419–444, (2012).

Zanchettin, D., Timmreck, C., Bothe, O., Lorenz, S.J., Hegerl, G., Graf, H.F., Lutherbacher,J., Jungclaus, J.H, Delayed winter warming: A robust decadal response to strong tropical volcanic eruptions. Geophys. Res. Lett. 40 (1), 204–209, (2013).

Zanchettin, D., Khodri, M., Timmreck, C., Toohey, M., Schmidt, A., Gerber, E. P., Hegerl, G., Robock, A., Pausata, F. S. R., Ball, W. T., Bauer, S. E., Bekki, S., Dhomse, S. S., LeGrande, A. N., Mann, G. W., Marshall, L., Mills, M., Marchand, M., Niemeier, U., Poulain, V., Rozanov, E., Rubino, A., Stenke, A., Tsigaridis, K., and Tummon, F.: The Model Intercomparison Project on the climatic response to Volcanic forcing (VolMIP): experimental design and forcing input data for CMIP6, Geosci. Model Dev., 9, 2701-2719, doi:10.5194/gmd-9-2701-2016, (2016).

Zanchettin, D., C. Timmreck, M. Toohey, J. H. Jungclaus, M. Bittner, S. J. Lorenz, A. Rubino. Clarifying the Relative Role of Forcing Uncertainties and Initial-Condition Unknowns in Spreading the Climate Response to Volcanic Eruptions. Geophys. Res. Lett. 46, 1602-1611, https://doi.org/10.1029/2018GL081018 (2019).

Zanchettin, D. Aerosol and Solar Irradiance Effects on Decadal Climate Variability and Predictability. Current Climate Change Reports, 3, 150, doi:10.1007/s40641-017-0065-y (2017).
Zanchettin, D., Timmreck, C., Khodri, M., Schmidt, A., Toohey, M., Abe, M., Bekki, S., Cole, J., Fang, S.-W., Feng, W., Hegerl, G., Johnson, B., Lebas, N., LeGrande, A. N., Mann, G. W., Marshall, L., Rieger, L., Robock, A., Rubinetti, S., Tsigaridis, K., and Weierbach, H.: Effects of forcing differences and initial conditions on inter-model agreement in the VolMIP volc-pinatubo-

1850 full experiment, Geosci. Model Dev., 15, 2265–2292, https://doi.org/10.5194/gmd-15-2265-2022,

1851 (2022).

1852

1853 Zhang, P., Wu, Y., Simpson, I. R., Smith, K. L., Zhang, X., De, B., & Callaghan, P. A stratospheric

1854 pathway linking a colder Siberia to Barents-Kara Sea sea ice loss. *Sci. Adv.*, *4*(7), eaat6025 (2018).

1855

1856 Zhang, R., Tian, W., Zhang, J., Huang, J., Xie, F., & Xu, M. The corresponding tropospheric

1857 environments during downward-extending and nondownward-extending events of stratospheric

1858 northern annular mode anomalies. *J. Clim*, *32*(6), 1857-1873 (2019).

1859

1860 Zhu, F., Emile-Geay, J., Anchukaitis, K. J., Hakim, G. J., Wittenberg, A. T., Morales, M. S., ... &

1861 King, J. A re-appraisal of the ENSO response to volcanism with paleoclimate data assimilation.

1862 *Nat. Commun.*, *13*(1), 747 (2022).

1863

1864 Zhuo, Z., Fuglestvedt, H. F., Toohey, M., and Krüger, K.: Initial atmospheric conditions control

1865 transport of volcanic volatiles, forcing and impacts, Atmos. Chem. Phys., 24, 6233–6249,

1866 https://doi.org/10.5194/acp-24-6233-2024, (2024).

1867

1868

1869

1870

1871

1872

Deleted: ,

Deleted: ,

Deleted: IR,

Deleted: KL,

Deleted: ,

Deleted: ,

Deleted:

Deleted: . 2018 Jul 25;

Deleted:):

Deleted: . doi: 10.1126/sciadv.aat6025. PMID: 30050990; PMCID: PMC6059732.

Formatted: Font: Italic

Formatted: Font: Italic

Formatted: Font: Italic

Deleted: (2022).

Deleted: *Nature communications*,

Deleted: .

Deleted: & Krüger

Deleted: . (2023).

Deleted: . *EGUsphere*, *2023*, 1-26.